Biomaterials 197 (2019) 305–316

Contents lists available at ScienceDirect

Biomaterials

journal homepage: www.elsevier.com/locate/biomaterials

EGFL7 regulates sprouting angiogenesis and endothelial integrity in a human blood vessel model

Ryo Usuba[a], Joris Pauty[a,b], Fabrice Soncin[b,c,d,**], Yukiko T. Matsunaga[a,b,c,*]

[a] Center for International Research on Integrative Biomedical Systems (CIBiS), Institute of Industrial Science, The University of Tokyo, 4-6-1 Komaba, Meguro-ku, Tokyo 153-8505, Japan
[b] LIMMS/CNRS-IIS (UMI 2820), Institute of Industrial Science, The University of Tokyo, 4-6-1 Komaba, Meguro-ku, Tokyo 153-8505, Japan
[c] CNRS/IIS/COL/Lille University SMMiL-E Project, CNRS Délégation Nord-Pas de Calais et Picardie, 2 rue de Canonniers, Lille, Cedex 59046, France
[d] Université de Lille, CNRS, Institut Pasteur de Lille, UMR 8161 - M3T, F-59000 Lille, France

HIGHLIGHTS

- We report new roles of EGFL7 in VEGF-A-stimulated endothelial cells using a human blood vessel-on-a-chip model.
- This study reveals EGFL7 interferes with tip/stalk regulation, endothelium integrity, and phosphorylation of VE-cadherin.
- The microvessel model demonstrated its capacity to enable elaborate observations for a better understanding of vascular biology.

ARTICLE INFO

Keywords:
Epidermal growth factor-like domain 7 (EGFL7)
Vascular endothelial growth factor (VEGF)
Endothelial cell junction
Vascular permeability
Angiogenesis
In vitro 3D model

ABSTRACT

Elucidating the mechanisms underlying sprouting angiogenesis and permeability should enable the development of more effective therapies for various diseases, including retinopathy, cancer, and other vascular disorders. We focused on epidermal growth factor-like domain 7 (EGFL7) which plays an important role in NOTCH signaling and in the organization of angiogenic sprouts. We developed an *EGFL7*-knockdown *in vitro* microvessel model and investigated the effect of EGFL7 at a tissue level. We found *EGFL7* knockdown suppressed VEGF-A-induced sprouting angiogenesis accompanied by an overproduction of endothelial filopodia and reduced collagen IV deposition at the basal side of endothelial cells. We also observed impaired barrier function which reflected an inflammatory condition. Furthermore, our results showed that proper formation of adherens junctions and phosphorylation of VE-cadherin was disturbed. In conclusion, by using a 3D microvessel model we identified novel roles for EGFL7 in endothelial function during sprouting angiogenesis.

1. Introduction

In adults, sprouting angiogenesis, the formation of new blood vessels from pre-existing ones, mainly takes place during tissue growth and repair. Sprouting angiogenesis also occurs in certain pathological conditions such as arthritis, retinal vascular diseases, and cancer [1]. In these contexts, angiogenesis leads to a disorganized network of blood vessels and disturbed vascular function, e.g., vascular permeability is increased due to defective blood vessel integrity [2]. In diabetic retinopathy, the increased permeability causes retinal blood vessels to bleed resulting eventually in retinal detachment [3,4].

At the molecular level, ischemia promotes sprouting angiogenesis by inducing the release of angiogenic factors from affected tissues [5,6]. Vascular endothelial growth factor (VEGF)-A is one of the main factors produced by ischemic tissues in normal and pathological conditions. It directly stimulates endothelial cells through its receptors (VEGFR) and co-receptors and induces the emergence of tip cells which extend filamentous, actin-rich protrusions (filopodia) and lead the angiogenic sprouts [7]. Endothelial stalk cells follow the leading tip cells and extend the sprout through proliferation [7]. These events have been documented mostly in the retinal vasculature, where it has been shown that the VEGFR and NOTHC signaling pathways are involved in the determination of the tip/stalk cell fate [8]. Yet, the underlying molecular and cellular mechanisms of sprouting angiogenesis are still not completely understood [9–11].

Epidermal growth factor-like domain 7 (EGFL7, VE-statin) was

* Corresponding author. Institute of Industrial Science, The University of Tokyo, 4-6-1 Komaba, Meguro-ku, Tokyo 153-8505, Japan.
** Corresponding author. CNRS UMI2820 LIMMS-IIS – SMMiL-E Project, IRCL, Place de Verdun, 59045 Lille, France.
E-mail addresses: fabrice.soncin@inserm.fr (F. Soncin), mat@iis.u-tokyo.ac.jp (Y.T. Matsunaga).

https://doi.org/10.1016/j.biomaterials.2019.01.022
Received 14 November 2018; Received in revised form 28 December 2018; Accepted 12 January 2019
Available online 14 January 2019
0142-9612/

initially identified as an endothelium-specific secreted factor mostly produced by blood vessel endothelial cells during development [12–14] and was later shown to play several functions in the vascular bed. Indeed, Egfl7 is involved in vascular lumen formation, blood vessel assembly, and morphogenesis in the zebrafish [14] and Xenopus [15]. EGFL7 affects human endothelial cell proliferation with opposite effects depending on the context; repression of *EGFL7* prevents proliferation in infected human umbilical vein endothelial cells (HUVEC) and in embryonic stem cells [16,17] whereas it promotes proliferation in human endothelial progenitor cells [18]. Moreover, secreted EGFL7 associates with the endothelial extracellular matrix (ECM), in particular with the elastic fibers [19,20]. EGFL7 has also been found to co-localize with fibronectin around blood vessels *in vivo* [14] and to interact with fibronectin *in vitro* [20]. At the molecular level, EGFL7 interferes with the NOTCH pathway – a major regulating pathway during sprouting angiogenesis – through direct interactions with NOTCH4, DLL4, and JAG1 [16]. Furthermore, EGFL7 promotes angiogenesis and cancer development in pre-clinical settings [21–23] by repressing endothelial cell activation and immune cell infiltration [24] through the down-regulation of the NF-κB pathway in endothelial cells [25]. EGFL7 is thus a promising target to study for a better understanding of mechanisms underlying endothelial cell functions.

The emergence of organ-on-a-chip technologies has attracted a great deal of attention [26,27]. These technologies aim at creating bioactive artificial tissues from cultured cells often employing microfluidic techniques. The 3D tissues are modeled from purpose-designed cells, e.g., human cells as a human tissue model. In this regard, an artificial microvessel has shown great potential to elucidate the vascular functions [28–30]. For example, the creation of a vascular network within a microfluidic channel has been achieved allowing observation of angiogenesis [28], and a single-vessel model has been developed for permeability measurement [29]. These techniques are promising not only for drug screening but also for basic biological studies because they allow multilateral analyses of blood vessels.

In order to analyze the roles of EGFL7 in VEGF-A-induced sprouting angiogenesis, vascular permeability, and endothelial junction formation, we fabricated an *in vitro* microvessel model and used *EGFL7* knocked-down human primary endothelial cells. We observed that *EGFL7* knockdown reduced sprouting angiogenesis while stimulating the emergence of filopodia from endothelial cells and increasing the permeability of the microvessels. *EGFL7* knockdown also significantly disrupted endothelial adherens junctions and reduced VE-cadherin phosphorylation in response to VEGF-A. These observations revealed new functions for EGFL7 in the regulation of endothelium integrity and response to angiogenic signals.

2. Materials and methods

2.1. Materials

Primary human umbilical vein endothelial cells (HUVEC) and Endothelial Cell Growth Medium-2 BulletKit (EGM-2) were from Lonza (Basel, Switzerland). Recombinant human VEGF-A_{165} and basic FGF were from R&D Systems (Minneapolis, MN, USA). 0.5 w/v% trypsin-5.3 mmol/L EDTA-4Na solution, 10× Dulbecco's phosphate buffered saline (−) (PBS), and 4% (w/w) paraformaldehyde were obtained from FUJIFILM Wako Pure Chemical Corporation (Osaka, Japan). Trypan Blue was from Nacalai Tesque (Kyoto, Japan). Lipofectamine RNAiMAX, OptiMEM, TRIzol®, Alexa Fluor 488 phalloidin, Alexa Fluor 568 phalloidin, Alexa Fluor 488 goat anti-rabbit, Alexa Fluor 568 goat anti-rabbit, Alexa Fluor 568 goat anti-mouse antibodies, and Hoechst 33342 were from Thermo Fisher Scientific (Waltham, MA, USA). siRNAs were from Dharmacon (Lafayette, CO, USA). ISOGEN was from Nippon Gene (Tokyo, Japan). Acupuncture needles (No.02, 0.20 mm × 30 mm, J type) were from Seirin (Shizuoka, Japan). Cellmatrix® Type I-A (3 mg/mL, pH 3) was from Nitta Gelatin (Osaka, Japan). Materials of the collagen buffer used for the neutralization of the collagen solution ($NaHCO_3$ 262 mM, HEPES 20 mM, NaOH 0.05 N. NaOH and $NaHCO_3$) but HEPES were from Kanto Chemical (Tokyo, Japan). HEPES, bovine serum albumin (BSA), Triton X-100, Fluorescein isothiocyanate-dextran (FITC-dextran, 70 kDa), and dextran from *Leuconostoc* spp. (Mr 450,000 − 650,000), and 10× Hanks' balanced salt solution were from Sigma-Aldrich (Saint Louis, MO, USA). Rhodamine-conjugated *Ulex europaeus* Agglutinin 1 lectin (UEA-1, 2 mg/mL) was from Vector Laboratories (Burlingame, CA, USA).

2.2. Cell culture

HUVEC were seeded on 21 cm^2 culture dishes, cultured at 37 °C in a humidified atmosphere of 5% CO_2/95% air, and used at 70–80% confluence. HUVEC were used between passages 4 to 7. Cells were rinsed once with PBS, incubated with 0.25% trypsin-EDTA solution for 3 min at 37 °C in 5% CO_2/95% air, and harvested in EGM-2. Cells were passed through a 35 μm cell strainer (Corning, NY, USA) to dissociate cell aggregates. The cells were then stained with Trypan Blue and live cells were counted using a hemocytometer.

2.3. Gene silencing by RNA interference

For transfection, HUVEC were seeded on 9.6 cm^2 well plates. After one day culture, cells were incubated with 50 nM of siRNA (siEGFL7, ON-TARGETplus Human EGFL7, 5′-GCAAGAAAGACUCGUGACU-3′) or non-targeting siRNA (siCtrl, ON-TARGETplus Non-targeting siRNA, 5′-UGGUUUACAUGUCGACUAA-3′) and Lipofectamine RNAiMAX in OptiMEM at 37 °C in 5% CO_2/95% air. After 6 h incubation, culture medium was replaced for EGM-2 and cells were cultured until the making of microvessels.

2.4. RT-qPCR analysis

Microvessels or leftover cells from the microvessel fabrication were used for RNA extraction and validation of EGFL7 silencing by RT-qPCR using TaqMan® technology. Cells were homogenized in TRIzol or ISOGEN, and the total RNA was extracted and reverse transcribed using High-Capacity cDNA Reverse Transcription Kit (Thermo Fisher Scientific). qPCR analyses were conducted using TaqMan Gene Expression Master Mix and the TaqMan probes of the tested genes (see Supplementary Table S1). Gene expression level was analyzed by $\Delta\Delta C_T$ method.

2.5. Preparation of the microvessel-on-a-chip

The polydimethylsiloxane (PDMS)-based chips (25 mm × 25 mm × 5 mm: width × length × height) which included needle inserting channels (300 μm in diameter) on both sides were used in this study. The fabrication method and validation have been previously described [31,32]. For fabrication of the microvessels, the PDMS chip was treated with O_2 plasma and sterilized by UV-light under a cell culture hood. An acupuncture needle (200 μm in diameter) was coated with PBS, 1% BSA, dried, and sterilized by UV-light exposure under a cell culture hood. The neutralized collagen solution was prepared on ice by mixing Cellmatrix® Type I-A collagen solution, 10× Hanks' buffer, and 10× collagen buffer (volume ratio 8:1:1) following manufacturer's protocol. Ice-cold neutralized collagen solution was then introduced into both wells and in the microvessel chamber; the BSA-coated acupuncture needle was inserted through the PDMS channel. Excessive collagen was carefully withdrawn from the wells. The device was then incubated at 37 °C in 5% CO_2/95% air for 60 min to allow the collagen to gel, resulting in the formation of a hollow channel upon withdrawal of the needle. HUVEC were harvested and resuspended in EGM-2 containing 3% dextran at a density of 1×10^7 cells/mL and 20,000 cells were loaded at each opening of the

collagen channel. Warmed medium (1 mL) was then added and the chip was further incubated for 4 h. Finally, the media was changed to FGF basic- and VEGF-A-free EGM-2, and the microvessels were maintained at 37 °C in 5% CO_2/95% air.

2.6. VEGF-A-induced sprouting angiogenesis

One-day after fabrication of the microvessels, culture medium was replaced with EGM-2 containing FGF basic (FGF-2) (5 ng/mL) and VEGF-A (1 ng/mL: low-VEGF or 10 ng/mL: high-VEGF). The medium was renewed every other day. Microscopic images were captured using an inverted phase-contrast microscope Observer Z1 (Carl Zeiss, GmbH, Oberkochen, Germany) equipped with a 20× objective lens (LD Plan-NeoFluar 20×/0.4 Korr Ph2 M27) and the ZEN 2 blue edition software (version 2.0.0.0, 64 bit, Carl Zeiss).

2.7. Image analysis for sprouting angiogenesis

Image analysis to assess responsiveness of the microvessel to VEGF-A was performed by the method of directional pixel variance as reported previously [32]. In this method, a value, which is calculated from phase-contrast images, indicates a roughness of microvessel edges. This method first measures the average pixel intensity and generates a translated profile which represents the theoretical image that would be obtained if the microvessel edges are straight. This profile is then deducted from the original image, thus highlighting areas where the pixel intensity varies from the theoretical image. This variance is then measured and normalized to compared the different microvessels.

2.8. OCT analysis

Label-free 3D imaging of the microvessel was performed by optical coherence tomography (OCT) using a Cell^3 iMager Estier (SCREEN, Kyoto, Japan) as reported previously [32,33].

2.9. Immunofluorescence

The cells were fixed with PBS, 4% (w/w) paraformaldehyde for 30 min, and permeabilized with PBS, 0.5% Triton X-100 for 10 min at 25 °C. Blocking in PBS, 1% BSA (blocking solution) was performed for overnight at 4 °C. Cells were then incubated overnight at 4 °C with a primary antibody in blocking solution; the used primary antibodies were against Claudin-5 (rabbit pAb, ab15106, Abcam, 1:200), Collagen IV (rabbit pAb, ab6586, Abcam, 1:200), Laminin (rabbit pAb, ab11575, Abcam, 1:100), vascular endothelial (VE)-cadherin (rabbit mAb, D87F2, Cell Signaling Technology, 1:200 / mouse pAb, sc-9989, Santa Cruz Biotechnology, 1:200), and ZO-1 (rabbit pAb, 40–2200, Thermo Fisher Scientific, 1:200). After several washes with PBS, cells were incubated for 2 h at 25 °C with a secondary antibody or fluorophore-labeled phalloidin for actin staining diluted in blocking solution (1:400). After washing with PBS, nuclei were stained by incubating the cells for 15 min at 25 °C with Hoechst 33342 in PBS (1:1000). After several washes with PBS, the chip was stored at 4 °C until imaging.

Images were taken using a confocal laser scanning microscope (CLSM, Laser Scanning Microscope 700, LSM 700, Carl Zeiss) equipped with a 40× water-immersion detection objective lens (LD C-Apochromat 40×/1.1 W Korr M27). Red fluorescence, green fluorescence, and Hoechst 33342 were detected using 555-, 488-, and 405-nm-wavelength lasers, respectively. Maximum intensity projection (MIP) images were obtained with the ZEN 2 blue edition software.

2.10. Permeability assay

The vessel permeability was measured as previously reported [31]. The microvessel was stained with 20 μg/mL rhodamine-conjugated UEA-1 in EGM-2 for 30 min at 37 °C. The microchip was then set up on a confocal microscope LSM700 (Carl Zeiss) in an incubation chamber that maintained 37 °C in a humidified 5% CO_2/95% air atmosphere (INU Incubation System for Microscopes–model WSKM, Tokai Hit Co., Fujinomiya, Japan). Images were taken using the CLSM equipped with a 10× observation lens (N-Achroplan 10×/0.25 M27). The rhodamine-conjugated UEA-1 staining was detected with the 555-nm-wavelength laser for focusing the center of the microvessel. After 15 μL of 100 μg/mL FITC-dextran (70 kDa) in EGM-2 solution were introduced, imaging was performed by detecting the fluorescence of FITC with the 488-nm-wavelength laser and an optical section of 77.8 μm. For quantifying the microvessel permeability, CLSM images taken one minute after introduction of FITC-dextran were used. The mean fluorescence intensity of FITC detected in collagen gel was measured within two regions of interest (0.2 mm × 2.5 mm, 0.5 mm^2) and summed.

2.11. Immune cell adhesion assay

THP-1 monocyte cells (1×10^6 cells) were labeled with 5 μM Calcein-AM (Thermo Fisher Scientific) for 30 min at 37 °C, washed three times and resuspended in RPMI with 10% FBS. THP-1 cells (1×10^5 cells) were then introduced into the microvessel and allowed to adhere on the endothelium for 30 min at 37 °C. Unattached cells were washed away three times. The attached cells were observed and counted using an inverted microscope Observer Z1 (Carl Zeiss).

2.12. Western-blotting for analyzing phosphorylation of VE-cadherin

Forty-eight hours after transfection, cells were starved for 4 h in EBM-2, 1% bovine serum albumin and stimulated with VEGF-A (100 ng/mL) for the indicated amount of time. Cells were lysed in PBS, 1% Igepal CA-630, 0.5% sodium deoxycholate, 0.1% SDS, complete inhibitors and PhosSTOP (Roche, Basel, Switzerland) for protein analysis.

Protein extracts were analyzed on 8% SDS-PAGE under reducing conditions and transferred onto polyvinylidene fluoride membranes (Immobilon P, Millipore, Burlington, MA, USA). Membranes were blocked in PBS, 0.1% Tween-20, 2% bovine serum albumin for 1 h at 25 °C, then incubated in the same buffer containing anti-phospho-VE cadherin (Tyr685) antibody (rabbit pAb, ab119785, Abcam, 1:1000), anti-phospho-VE-cadherin (Tyr731) antibody (rabbit pAb, 44-1145G, ThermoFisher, 1:1000), anti-phospho-VE-cadherin (Tyr658) antibody (rabbit pAb, 44-1144G, ThermoFisher, 1:1000), and incubated with a corresponding secondary antibody, anti-rabbit-HRP (goat IgG, #7074, Cell Signaling Technology, 1:10000). Detection was performed using ECL-Prime (#RPN2232, GE-Healthcare, Chicago, IL, USA) and chemiluminescence detected by film exposure and using a Luminescent image system (LAS3000, Fujifilm, Tokyo, Japan). For analysis of total VE-cadherin levels, membranes were stripped by treatment using Reblot Mild (Millipore) for 20 min at 25 °C before blocking and incubating with anti-VE-cadherin (C-19) (goat pAb, sc-6458, Santa Cruz Biotechnology, 1:1000) and a secondary antibody, anti-goat-HRP (donkey IgG, #250C, Jackson 1:10000) in similar conditions.

2.13. Statistical analysis

All data are presented as mean ± standard deviation (S.D.) of at least three experiments. Significance was determined by using Student's *t*-test or Welch's *t*-test to compare two groups, and One-way ANOVA followed by Tukey's post hoc test to compare more than two groups. Difference with P values < 0.05 were considered significant.

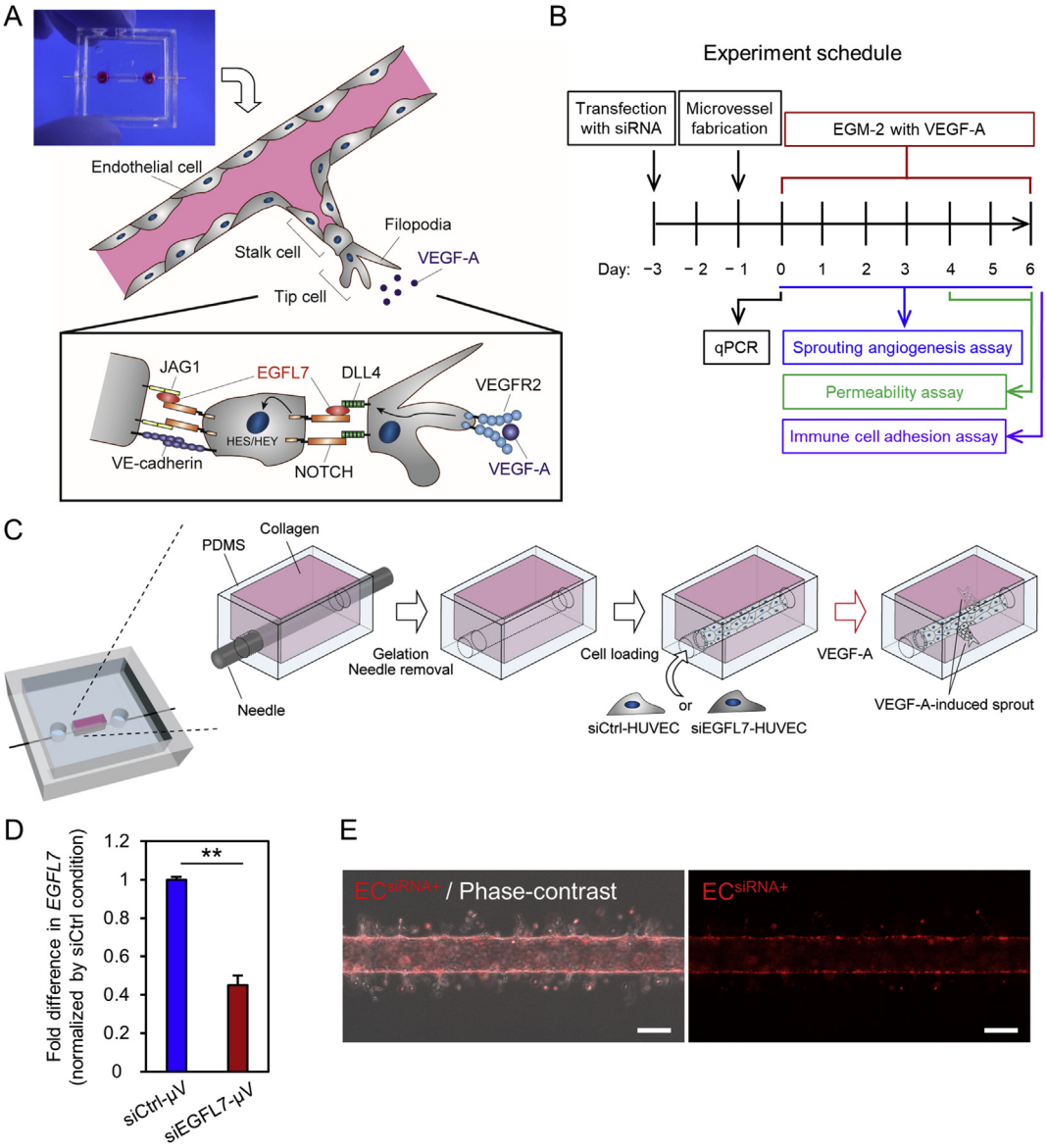

Fig. 1. *In vitro EGFL7* knockdown microvessel model. (A) Conceptual diagram showing VEGF-A-induced sprouting angiogenesis on a chip, and the molecular pathways involved in tip/stalk cell selection and maintenance. During sprouting angiogenesis, VEGF-A binds its receptor, VEGFR-2 on endothelial cells (EC), activating EC's filopodia formation and migration (tip cell). Tip cell expresses DLL4, which activates the NOTCH pathway in the adjacent EC. Upon activation, the intracellular domain of NOTCH enters the nucleus and induces the expression of genes such as HES and HEY orienting the EC to a stalk cell fate, which is less responsive to VEGF-A. Meanwhile this stalk cell also orients neighboring EC to a stalk cell fate by NOTCH-JAG1 binding. Stalk cells proliferate and form cell junctions mediated by VE-cadherin. (cf. text for details). (B) Timeline of the experiments in this study. (C) Fabrication process for the *EGFL7* knockdown microvessel model (cf. text for details). (D) Knockdown efficiency of *EGFL7* in microvessels at day 0 (1 day after microvessel fabrication, 3 days after transfection). Relative proportion of *EGFL7* compared to the beta-2 microglobulin gene as quantified by RT-qPCR; the value was normalized to the siCtrl condition and is expressed as a fold difference. RNA was extracted from 3 pooled microvessels. Error bars = S.D. $^{**}p < 0.01$. (E) Microvessel fabricated with a fluorescent siRNA showing that most of endothelial cells contain siRNA. Scale bar: 200 μm.

3. Results

3.1. *EGFL7* knockdown alters sprouting angiogenesis in the microvessel model

In order to study the effects of *EGFL7* knockdown in the context of VEGF-A-induced sprouting angiogenesis using an *in vitro* microvessel model (Fig. 1), we first determined culture conditions which allowed a clear transition from non-induced to VEGF-A-induced sprouting angiogenesis. Microvessels were cultured in EGM-2 containing VEGF-A (0–50 ng/mL) and FGF-2 (0 or 5 ng/mL) (Fig. S1). Sprouting angiogenesis was observed when microvessels were cultured in the presence of 10 or 50 ng/mL VEGF-A, regardless of the presence of FGF-2. On the other hand, stable non-sprouting vessels were obtained in culture containing less than 2 ng/mL VEGF-A, although FGF-2 was needed for cell survival in these conditions. Based on these observations, we defined "low-VEGF" conditions as 1 ng/mL VEGF-A for obtaining a quiescent microvessel and "high-VEGF" conditions as 10 ng/mL VEGF-A for inducing sprouting angiogenesis.

To produce the *EGFL7*-knockdown microvessels, HUVEC were transfected either with a non-targeting control siRNA (siCtrl) or with a siRNA specifically targeting EGFL7 (siEGFL7) and which did not affect miR-126 or miR-126-5p expression [25], at a transfection efficiency of more than 95% and a knockdown efficiency of 70 ± 2.9% (Fig. S2). Transfected HUVEC were seeded into a microfabricated 200-μm-diameter collagen gel channel and allowed to form an endothelium. siCtrl-

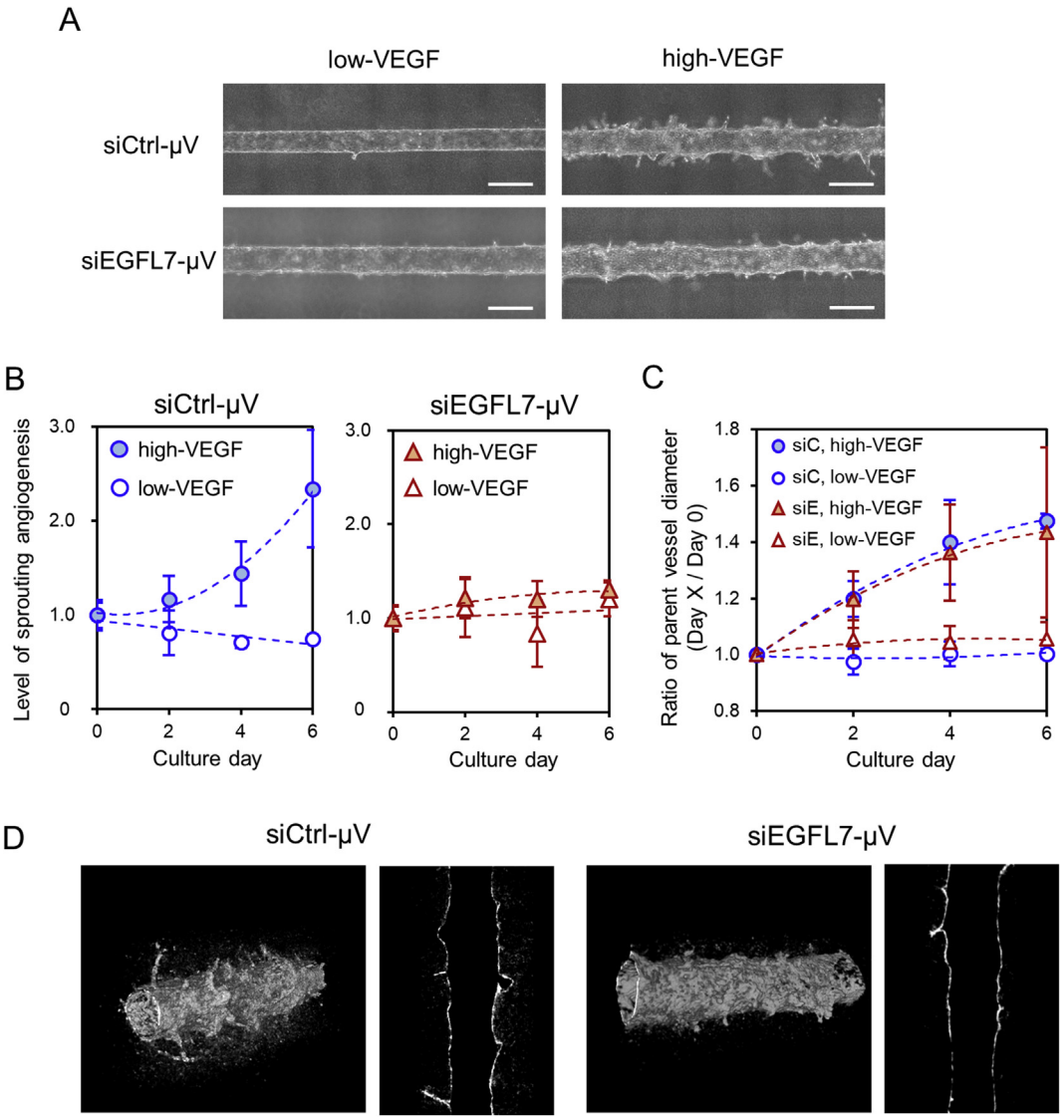

Fig. 2. Effect of *EGFL7* deficiency on microvessels activated by VEGF-A. (A) Phase-contrast images of microvessels at day 6. The microvessels were cultured under low-VEGF (1 ng/mL) or high-VEGF (10 ng/mL) conditions. Scale bar: 500 μm. (B) Level of sprouting angiogenesis calculated by averaged directional pixel variance. $n \geq 8$. Error bars = S.D. The difference between siEGFL7-μV and siCtrl-μV at day 6 under high-VEGF had $p < 0.05$. (C) Change in parent vessel diameter of the microvessels of siCtrl (siC) and siEGFL7 (siE). $n \geq 8$. Error bars = S.D. (D) 3D and sectioned images of microvessels with induced sprouting angiogenesis at day 6 observed by OCT.

transfected microvessels (siCtrl-μV) and siEGFL7-transfected microvessels (siEGFL7-μV) were successfully formed and *EGFL7* knockdown was maintained (reduction of 55 ± 5.0%, Fig. 1D). At day 6 (7 days after microvessel fabrication and 9 days after transfection), the reduction of *EGFL7* was still of 11 ± 4.1% (Fig. S2), which indicated that *EGFL7* repression was maintained at least during the initial period of sprouting angiogenesis. Furthermore, transfection with a fluorescent siRNA showed that siRNA-transfected cells homogeneously contributed to the 3D endothelium (Fig. 1E).

We then demonstrated VEGF-A-induced sprouting angiogenesis on both siCtrl-μVs and siEGFL7-μVs up to 6-days of culture. In high-VEGF conditions, siCtrl-μVs showed a large number of sprouts, as seen in our previous study [32]. Interestingly, the siEGFL7-μVs showed fewer sprouts of shorter length, although endothelial cells did respond to VEGF-A as indicated by the wavy edge of microvessels (Fig. 2A, Fig. S3). To quantify the sprouting angiogenesis, phase-contrast images were analyzed using the directional pixel variance method [32]. This method calculates a value for roughness of microvessel edges associated with the presence of sprouts. To appreciate the roughness variation through over time, the ratio of the value relative to day 0 was calculated as a level of sprouting angiogenesis. In siCtrl-μVs, low-VEGF conditions induced a level of sprouting angiogenesis which remained relatively stable between days 0–6 ranging from 1.0 to 0.75 (Fig. 2B), whereas high-VEGF conditions increased the level from 1.0 to 2.3. On the other hand, the measured levels of sprouting angiogenesis remained relatively low and stable in siEGFL7-μVs independently of the concentration of VEGF-A. Upon VEGF-A stimulation, we also observed a diameter increase of the parent microvessel which may reflect proliferation of the endothelial cells (Fig. 2C). There were no significant differences in diameter variation between siCtrl-μVs and siEGFL7-μVs under similar VEGF-A conditions.

3D imaging by optical coherence tomography (OCT) allowed a more precise structural observation of microvessels [33]. This confirmed that the sprouts were induced in both siCtrl-μV and siEGFL7-μV, and that siEGFL7-μV showed short sprouts (Fig. 2D). Moreover, the sectioned OCT images indicated the smaller volume of the induced sprouts in siEGFL7-μV.

Taken together, these results indicated that *EGFL7* knockdown

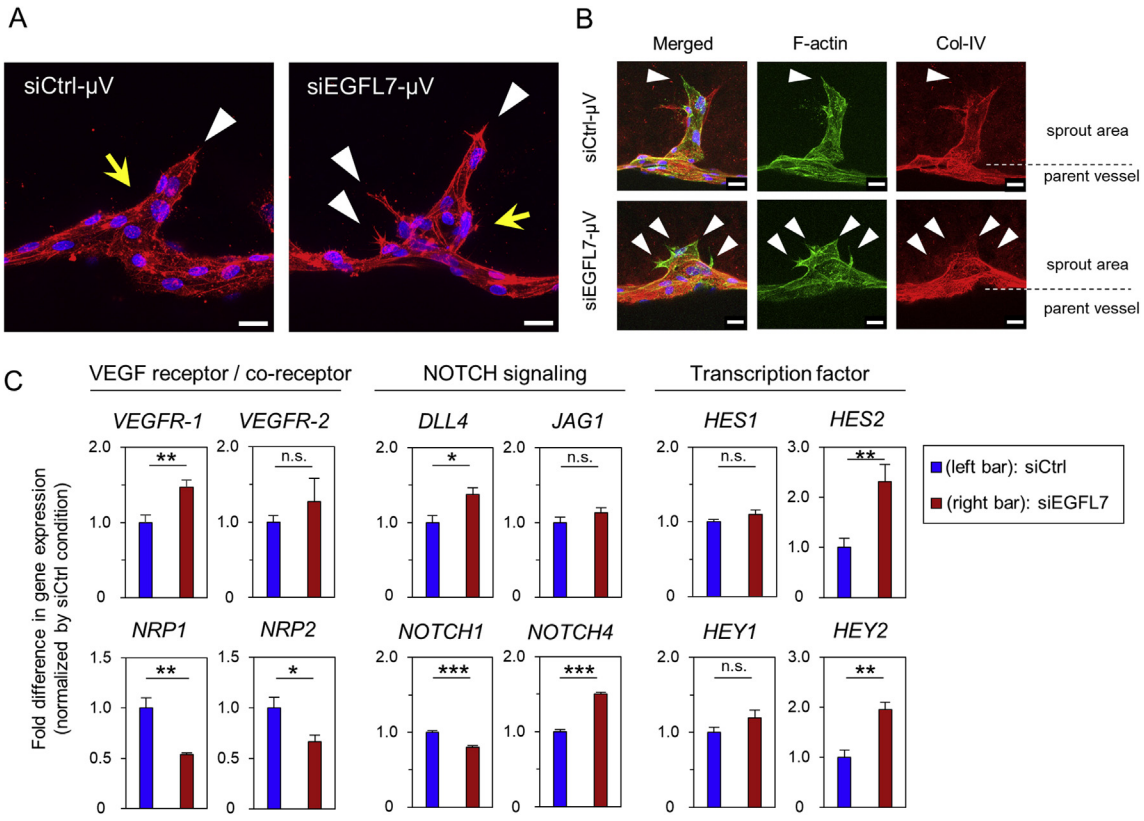

Fig. 3. Disturbance of tip cells in VEGF-induced sprouts. (A) Characterization of tip cell formation in VEGF-A-induced sprouts visualized by immunofluorescence under CLSM (red: F-actin, blue: nuclei). White triangles and yellow arrows indicate tip-like cell showing filopodia and stalk-like cells, respectively. Scale bar: 20 μm. (B) Characterization of ECM protein deposition in angiogenic sprouts visualized by immunofluorescence under CLSM. White triangles indicate the area losing collagen IV (Col-IV). Scale bar: 20 μm. (C) Gene expression of sprouting angiogenesis-related genes. Relative proportion of genes compared to the beta-2 microglobulin gene as quantified by RT-qPCR; the value was normalized to the siCtrl condition and is expressed as a fold difference. Measures were from 3 independent 2D cultures of one experiment. Error bars = S.D. $*p < 0.05$; $**p < 0.01$; $***p < 0.001$. (For interpretation of the references to color in this figure legend, the reader is referred to the Web version of this article.)

specifically inhibited sprouting angiogenesis without preventing an apparent response of endothelial cells to VEGF-A.

3.2. *EGFL7* knockdown induces the emergence of filopodia-rich cells

We then compared the sprout morphologies between siCtrl-μV and siEGFL7-μV, since, based on the literature and above observations, we suspected that the absence of EGFL7 would disrupt the relationship between endothelial cells. Immunostaining was performed to discriminate between tip and stalk cells in the induced sprouts (Fig. 3A, Fig. S4). In siCtrl-μV, single tip cells were clearly visible at the leading edges of sprouts whereas stalk cells were organized behind the single tip cells. On the other hand, in siEGFL7-μV, several cells showed filopodia protrusions along single sprouts (white arrow in Fig. 3A), suggesting the concomitant emergence of several tip cells within one single sprout. Interestingly, overproduction of the filopodia was observed only around the sprouting area, and not elsewhere along the parent vessel endothelium. This suggested that *EGFL7* knockdown disrupted the signaling pathways regulating the tip/stalk cell interactions within an induced sprout rather than the pathways involved in tip cell selection within a parent vessel [34].

Next, we performed immunostaining of collagen IV and laminin (Fig. 3B, Fig. S5). Collagen IV was clearly detected along the whole sprout in siCtrl-μV except at the tip cell. On the other hand, collagen IV was lacking in several areas of a sprout in siEGFL7-μV (white triangle, Fig. 3B). Similarly, laminin staining was detected along the whole sprout except in the filopodia of tip-like cells in both siCtrl-μV and siEGFL7-μV (Fig. S5). Similar results were also found in immunohistochemistry observations of the microvessels (Fig. S6).

Endothelial tip/stalk selection and maintenance is mainly regulated by the VEGFR and DLL4-NOTCH pathways [8]. To check whether *EGFL7* knockdown disturbed these signaling pathways in high-VEGF conditions, as suggested by the above observations and previous reports [16,35], the levels of expression of genes involved were compared by RT-qPCR (Fig. 3C). We noted that *VEGFR-1* expression levels were upregulated when *EGFL7* was repressed, while the VEGF-A co-receptors *NRP1* and *NRP2* were downregulated. Regarding NOTCH pathway, *DLL4*, *NOTCH4*, *HEY2*, and *HES2* expression levels were found to be upregulated in siEGFL7-HUVEC while the expression levels of *JAG1*, *HES1*, and *NOTCH1* did not seem to be strongly affected.

These results suggested that the downregulation of *EGFL7* disrupted the balance of expression of genes involved in the regulation of tip/stalk cell fate along the interdependent VEGFR and NOTCH signaling pathways, resulting in a decrease rate of sprouts and increased number of filopodia in our model.

3.3. *EGFL7* knockdown impairs barrier function in the microvessel model

Since there is a close relationship between angiogenesis inhibition and vessel permeability [1,32,36], we assessed whether repression of *EGFL7* would affect the barrier function. Indeed, the microvessel model used is well suited to investigate changes in endothelial permeability along the initial parent vessel [31,32]. FITC-labeled 70 kDa dextran perfusion was used to visualize vessel leakages induced in high-VEGF conditions (Fig. 4A). siCtrl-μVs showed leakages starting from defined points that could be explained by the expected effect of VEGF-A, which

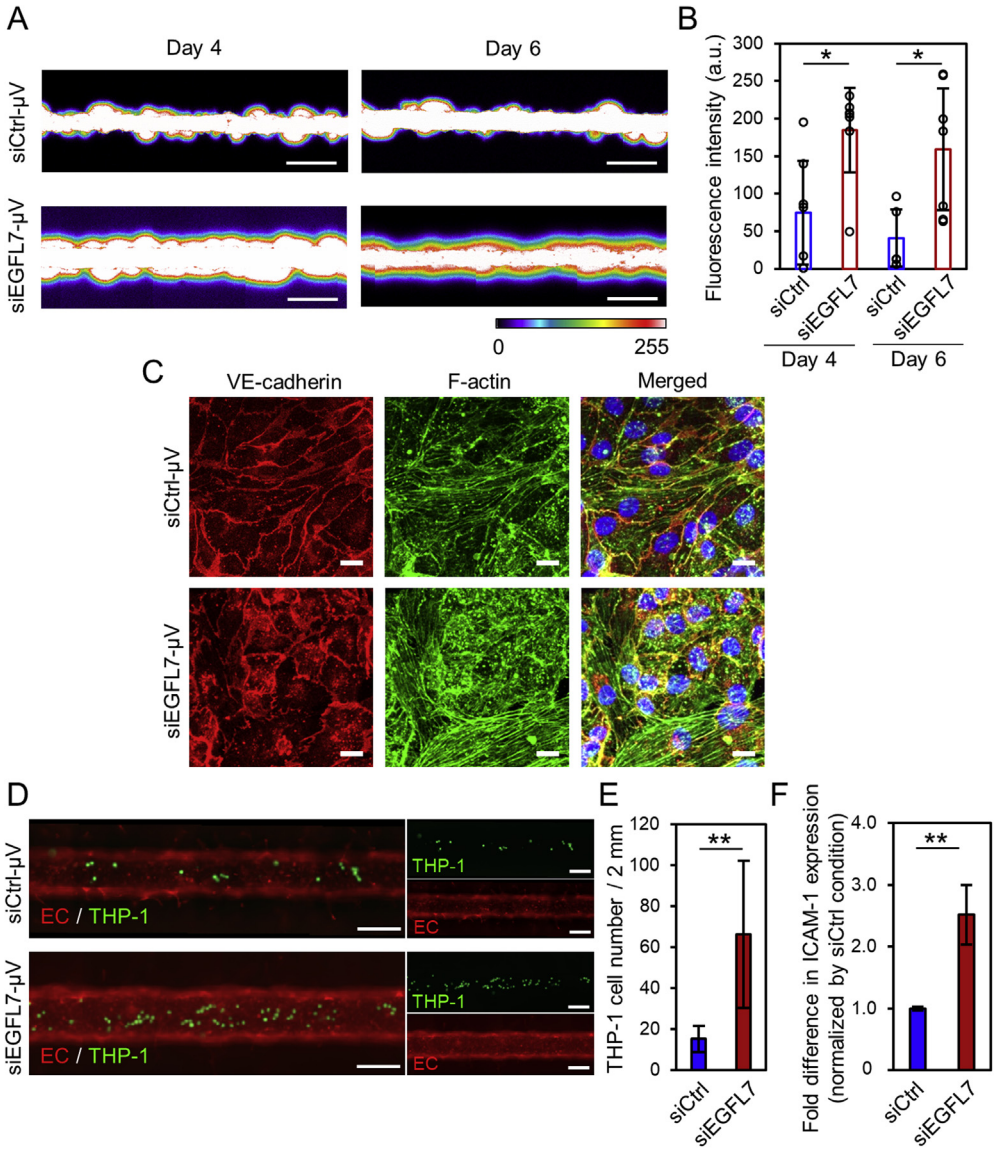

Fig. 4. Endothelial barrier function of *EGFL7* knockdown microvessels. (A) Fluorescence image of permeability assay on the microvessels at days 4 and 6 under high-VEGF conditions. FITC-labeled 70 kDa dextran was introduced into the microvessels to characterize endothelial barrier function. Scale bar: 500 μm. (B) Quantification of the leakage of 70 kDa dextran into the collagen gel area (outside the vessel). The region of interest (ROI: 0.2 × 2.5 mm) was set on each side of the microvessel to measure the average fluorescence intensity value. $n = 7$. (C) Immunofluorescence images of the bottom surface of the microvessels at day 4 observed by CLSM. Adherens junctions (VE-cadherin) and cytoskeleton (F-actin) were analyzed. Confocal images are maximum intensity projection from Z-stack images. Scale bar: 20 μm. (D) THP-1 adhesion assay in the microvessel model. For visualization, THP-1 cells and endothelial cells (EC) were labeled with Calcein-AM and UEA-1, respectively. Scale bar: 200 μm. (E) Quantification of THP-1 cells adhered onto the endothelium. $n = 8$. (F) Relative proportion of *ICAM-1* compared to the beta-2 microglobulin gene as quantified by RT-qPCR; the value was normalized to the siCtrl condition and is expressed as a fold difference. Error bars = S.D. $^{*}p < 0.05$; $^{**}p < 0.01$.

increases permeability. However, siEGFL7-μVs were leakier at days 4 and 6. This difference in leakage indicated that *EGFL7* knockdown affected the integrity of the endothelium. Therefore, EGFL7 itself is important for maintaining endothelial integrity. Quantification of the observations confirmed that siEGFL7-μVs were 2.5-fold and 3.9-fold more permeable than siCtrl-μVs at days 4 and 6, respectively (Fig. 4B).

VE-cadherin is one of the main endothelial junction molecules involved in the maintenance and control of endothelial cell integrity in the context of the barrier function [37,38]. Microvessels were therefore stained for VE-cadherin and F-actin and observed by confocal observation (Fig. 4C). siCtrl-μV showed typical adherens junctions characterized by distinct, continuous VE-cadherin staining at cell–cell contacts, colocalizing with F-actin. On the other hand, VE-cadherin staining in siEGFL7-μV showed a discontinuous pattern with a lack of signals in many areas along the cell–cell contacts, indicating that the integrity of adherens junctions was disrupted when *EGFL7* was repressed, as results from the permeability assays suggested. In addition, actin stress fibers were observed in the endothelium of siEGFL7-μV, notably in the area of cell–cell contacts devoid of VE-cadherin signal.

An increase in endothelial permeability associated with a weakening of cell–cell junctions is a phenotype often observed in inflammatory conditions [39,40]. In these conditions, immune cells are capable of adhering to endothelium through the activation of endothelial adhesion molecules, such as Intercellular adhesion molecule-1 (ICAM-1). Since EGFL7 is known to be associated with inflammation in endothelium [25,41], we then assessed THP-1 (a human monocytic cell line) cell adhesion onto the endothelium in the microvessel model. THP-1 cells were loaded into siCtrl-μVs and siEGFL7-μVs, and allowed to attach to the endothelium. In siEGFL7-μV, significantly more THP-1 cells attached onto the vessel than in siCtrl-μV (Fig. 4D and E). Furthermore, in siEGFL7-HUVEC the expression level of *ICAM-1* was double that in siCtrl-HUVEC (Fig. 4F). Therefore, these results confirmed that siEGFL7-μV was in a *de novo* inflammatory state.

Taken together, these results demonstrated that *EGFL7* knockdown caused the inflammation and loss of integrity of the endothelial monolayer.

3.4. *EGFL7* knockdown cells exhibit disturbed endothelial cell junctions

As we observed a clear loss of endothelium integrity in siEGFL7-μV, we decided to further investigate the underlying mechanism. VE-cadherin and ZO-1/Claudin-5 are components of the endothelial adherens and tight junctions, respectively; their proper expression and localization at the endothelial junction directly regulate vessel permeability [42,43]. siCtrl- and siEGFL7-transfected HUVEC were cultured as a confluent monolayer in presence of VEGF-A (10 ng/mL), and VE-

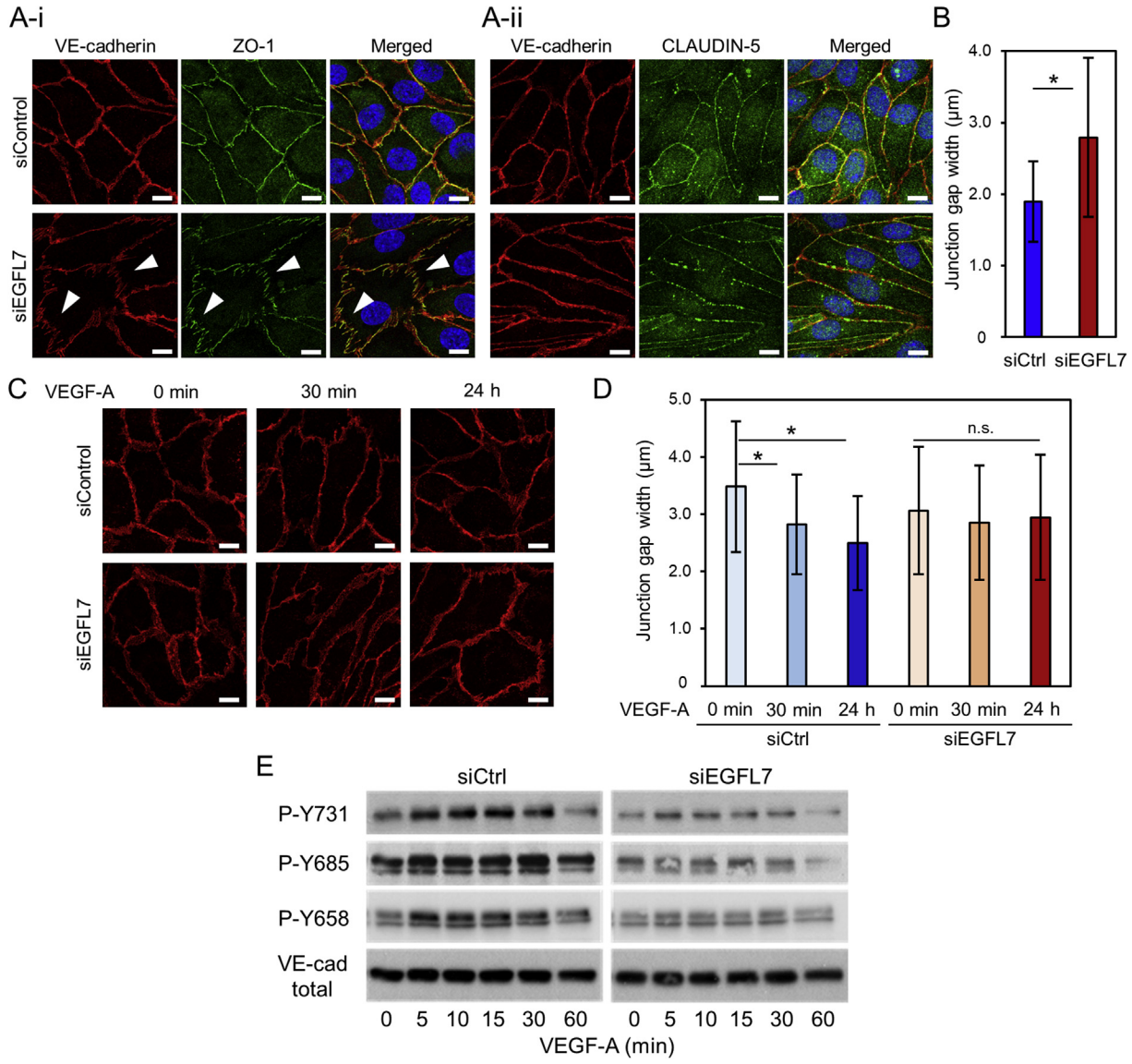

Fig. 5. Disturbance of adherens junctions in *EGFL7* knockdown endothelial cells. (A) CLSM images of endothelial monolayer with immunostained junction molecules: VE-cadherin (adherens junctions: red) and ZO-1 (i) or Claudin-5 (ii) (tight junctions: green). The endothelial monolayer was cultured on a glass surface coated with collagen I-A under high-VEGF conditions. White arrow heads indicate a ruffled structure. Scale bar: 10 μm. (B) Quantification of junction gap width measured using the fluorescence images from VE-cadherin staining. $n = 45$. (C, D) VE-cadherin time-dependent changes in response to VEGF-A (10 ng/mL): immunofluorescence images by CLSM of the endothelial monolayer (C) and quantification of junction gap width (D). $n = 45$. (E) Time-dependent phosphorylation of VE-cadherin in response to VEGF-A (100 ng/mL). Western blot of VE-cadherin and phosphorylation on tyrosine residues. Error bars = S.D. $^*p < 0.05$. (For interpretation of the references to color in this figure legend, the reader is referred to the Web version of this article.)

cadherin, ZO-1, and Claudin-5 were assessed by immunofluorescence (Fig. 5A). siCtrl-HUVEC retained both typical adherens junctions and tight junctions with a regular and continuous distribution along cell borders. However, the siEGFL7-HUVEC monolayer showed ruffled and widened VE-cadherin staining; meanwhile ZO-1 staining aligned with the shape of the VE-cadherin staining but did not show widening. When analyzing the merged images, VE-cadherin colocalized with ZO-1 in siCtrl-HUVEC (yellow signal in Fig. 5A–i), whereas signals were separated in siEGFL7-HUVEC. Claudin-5 staining in siEGFL7-HUVEC appeared punctuated, indicating immature tight junctions (Fig. 5A–ii). Quantification of the junction widths from the VE-cadherin staining confirmed a significant increase in siEGFL7-HUVEC as compared to siCtrl-HUVEC (Fig. 5B). Moreover, VE-cadherin was clearly disrupted or missing in some areas of the siEGFL7-HUVEC monolayer (white triangles in Fig. 5A–i). This pattern of jagged and missing staining of VE-cadherin was similar to previously reported observations associated with increased permeability [31,44].

We also examined the kinetics of VE-cadherin redistribution in response to VEGF-A in similar 2D conditions. The transfected HUVEC were starved in a VEGF-A-free medium and then stimulated with 10 ng/mL VEGF-A for up to 24 h. In the absence of VEGF-A, both siCtrl-HUVEC and siEGFL7-HUVEC showed thick and jagged VE-cadherin staining (Fig. 5C). When cells were stimulated with VEGF-A, siCtrl-HUVEC retained the jagged VE-cadherin after 30 min of VEGF-A stimulation, but then showed a thinner staining and more regular VE-cadherin after 24 h. On the other hand, in siEGFL7-HUVEC, VE-cadherin maintained a ruffled-shape and was missing in some areas for the whole duration of the experiment. Quantification of these observations confirmed time-dependent changes in VE-cadherin (Fig. 5D). These observations indicated that *EGFL7* knockdown interfered with the formation/rearrangement of adherens junctions following VEGF-A stimulation.

Finally, in an attempt to further understand the molecular effects of EGFL7 on the adherens junctions and regulation of VE-cadherin activity, we analyzed the time-dependent phosphorylation status of VE-cadherin in response to VEGF-A. In siCtrl-HUVEC, western-blotting analysis showed a clear increase in VE-cadherin phosphorylation on Tyrosines 658, 685, and 731 (Y658, Y685, Y731) in response to VEGF-A, with levels resuming initial values after 1 h (Fig. 5E). This was in good agreement with previously published observations which reported a similar time-course of phosphorylation/dephosphorylation on these residues [45,46]. In contrast, siEGFL7-HUVEC already exhibited a strikingly low level of basal phosphorylation on Y685 in the absence of VEGF-A treatment, and an almost complete absence of increase of phosphorylation on all three tyrosine residues following VEGF-A stimulation. Total VE-cadherin content was stable during these time-course stimulations. These results showed that EGFL7 is necessary for the proper regulation of phosphorylation of VE-cadherin in response to VEGF-A stimulation.

These data describing the impaired cell–cell junctions in siEGFL7-HUVEC suggested that repression of *EGFL7* altered endothelial monolayer integrity by interfering with the proper phosphorylation of VE-cadherin, resulting in the loss of regular formation of VE-cadherin-associated adherens junctions.

4. Discussion

In this study, we used a microvessel-on-a-chip to demonstrate the pertinence of such approach to unravel the molecular mechanisms involved in blood vessel emergence. We investigated the effects of *EGFL7* deficiency on 3D sprouting angiogenesis and endothelial barrier function using an *in vitro* human microvessel model which led to demonstrate new functions of EGFL7 on tip cell emergence and on the regulation of the endothelial barrier (Fig. 6A).

During the setup of conditions for inducing sprouting angiogenesis in this microvessel model, we observed that endothelial sprouting from the initial vessel necessitated two angiogenic factors, i.e. VEGF-A and FGF-2. VEGF-A is the major inducer of angiogenesis *in vivo* during development and the main signal to which quiescent endothelial cells respond when stimulated to form an angiogenic sprout [47]. In our setting, HUVEC responded to VEGF-A by angiogenic morphogenetic events which closely matched those observed *in vivo*, including the formation of tip-like cells with extended filopodia located at the migrating front, and basal stalk-like cells which form the main body of the sprouts and the vascular lumen [48]. On the other hand, FGF-2 was also necessary to the establishment of parent microvessel, as expected since it is known to promote endothelial proliferation and survival [49]. In low VEGF-A condition, we noted that FGF-2 was still needed to maintain the integrity of the parent vessel. This is in line with the fact that FGF signaling is actually involved in the maintenance of endothelial junction integrity, as disrupting FGFR1 signaling leads to a loss of endothelial cell contacts, a disturbance of VE-cadherin distribution *in vivo*, and an increase in vascular permeability [50]. Overall, we showed that the formation and the maintenance of the parent vessel and the sprouting process in our 3D microvessel depend on similar signals to those needed to form angiogenic sprouts *in vivo*, thus further validating our system and allowing us to study the molecular processes involved in blood vessel integrity and angiogenic sprouting.

Although EGFL7 has been characterized more than a decade ago as a gene specifically expressed by endothelial cells [12–14], its roles in angiogenesis *per se* are not clear yet. Repression of *EGFL7* in HUVEC suppressed endothelial cell sprouting in a fibrin gel bead assay, wherein defects were attributed to a deficit in cell adhesion [15]. In addition, in an embryonic body model using *Egfl7* knocked-down mouse cells, the formation of abnormal sheet-like endothelial structures and a deficit in endothelial cell junction markers was observed, although no major differences in angiogenic sprouting were found [17]. These observations suggested that EGFL7 participated in the induction of sprouting endothelial cells. Here, we observed that *EGFL7* repression induced the formation of a leakier parent vessel and, upon VEGF-A stimulation, reduced the frequency of emerging angiogenic sprouts. This therefore confirmed that endogenous EGFL7 participates in promoting angiogenic sprouting in response to VEGF-A. Based on the previous studies and our results, it also suggests that these effects of *EGFL7* deficiency are context-dependent, depending on the microenvironment, including growth factor levels. This may actually explain why endothelial colony forming cells (ECFC) and HUVEC respond differently to *EGFL7* repression [16,18] since ECFC are heterogeneous and immature endothelial cells which exhibit higher tube-forming capacity and tip cell gene expression upon VEGFR2 signaling. Interestingly, when co-cultured with HUVEC, ECFC participate more frequently to tip cells at the expense of HUVEC [51,52], clearly indicating that these two cell types show different behavior in response to VEGF-A.

Regarding the role of EGFL7 in the emergence of tip cells, we found that filopodia-rich, tip-like cells lacking basal collagen IV emerged more profusely around sprouts of *EGFL7* knockdown vessels. This correlates to previous observations reporting that tip cells have little collagen IV and EGFL7 deposition at their basal side [53,54]. The emergence of tip and stalk cells during sprouting angiogenesis is regulated by several factors. Briefly, VEGF-A stimulation of quiescent endothelial cells activates VEGFR-2, stimulates endothelial migration and filopodia formation and induces the expression of the NOTCH ligand DLL4 in the becoming tip cells. The VEGFR-2 co-receptor NRP1 further enhances the activation of VEGFR-2 in these cells [55]. DLL4 expression by tip

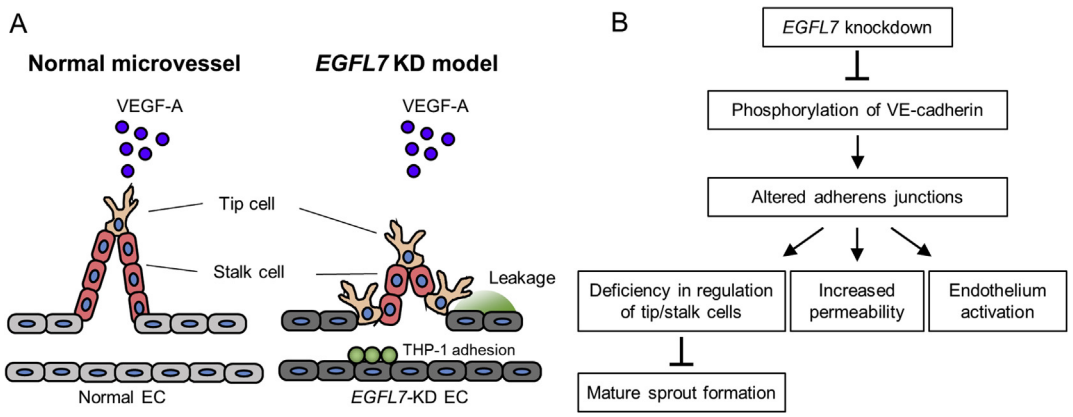

Fig. 6. Summary of the present study and proposed hypothesis for the roles of EGFL7 in sprouting angiogenesis and barrier function. (A) Schematic illustration of the phenomena observed in the microvessel model. (*EGFL7* KD: *EGFL7* knockdown, EC: endothelial cell). (B) Chart proposing how the effects of *EGFL7* knockdown observed in the present study could be interconnected.

cells stimulates the NOTCH pathway in neighboring endothelial cells, thus preventing those from engaging in the tip cell phenotype [56], decreasing VEGFR-2 and NRP1 but increasing VEGFR-1, and rendering these stalk cells less responsive to VEGF-A. Tip cell fate is not definitively acquired as endothelial cells compete for the tip cell position at the leading edge of sprouts; endothelial cells with the highest VEGFR-2 and lowest VEGFR-1 levels gain the tip cell position [57]. Here, we observed that repressing *EGFL7* in endothelial cells reduces the numbers of emerging angiogenic sprouts while, at the same time, increasing the numbers of filipodia-rich cells at the sides and bases of the sprouts. This shows that endogenous EGFL7 is actually promoting the angiogenic sprouting and repressing the formation of filopodia. Filopodia formation is actually not necessary to the guidance of tip cells and the formation of intersegmental blood vessels in zebrafish [58] and the effects of EGFL7 on filopodia formation and on sprouting events might therefore be taken as independent events. Regarding the reduced formation of angiogenic sprouts in siEGFL7-microvessels, we observed that *EGFL7* repression led to an increase in *VEGFR-1* expression while *VEGFR-2* expression levels were not significantly changed. Therefore, repressing *EGFL7* tilts the balance of expression of these receptors. This balance is of utmost importance to the tip cell selection and sprouting angiogenesis, and the relative levels of expression of *VEGFR-1* and *VEGFR-2* in endothelial cells direct the competition for the tip cell position; cells with higher *VEGFR-2* taking the leading position [57]. Furthermore, repression of *EGFL7* also reduced the expression levels of *NRP1* and therefore depleted cells from a major co-activator of VEGFR-2 which also contributes to the tip cell fate [55]. Accordingly, the repression of *EGFL7* resulted in the activation of the NOTCH pathway, increasing the expression levels of NOTCH target genes such as *HES2* and *HEY2*. All these observations made by repressing *EGFL7* concur to show that endogenous EGFL7 actually favors the tip cell fate by maintaining low expression levels of VEGFR-1, high expression levels of NRP1 thus allowing high activation levels of VEGFR-2 in response to VEGF-A and by maintaining low activation of the NOTCH pathway. Several questions remain unanswered as, so far, we have studied the expression levels of these genes in the global endothelial population while they are certainly finely tuned at the cell level within the angiogenic sprouts. More molecular analyses at the individual cell level are therefore required in order to better understand the role of EGLF7 in this morphogenetic process.

Another original observation made in this study was the fact that repressing *EGFL7* disturbed the endothelial monolayer integrity and directly affected VE-cadherin localization and phosphorylation. VE-cadherin is the main adhesion molecule of endothelial adherens junctions, directly involved in the maintenance of endothelium integrity [59–61] and phosphorylation of its cytoplasmic domain on various residues affects endothelial monolayer integrity [62]. The phosphorylation status of VE-cadherin, especially on its tyrosine residues, has been associated with several effects. Notably, VE-cadherin is strongly phosphorylated in HUVEC in response to VEGF-A stimulation [39]. *In vivo*, VEGF-A and T-cell binding onto endothelial cells induces the phosphorylation of Y685 [63]. Nevertheless, tyrosine-to-phenylalanine mutation of VE-cadherin Y685 knock-in mice showed an increase in VEGF-induced permeability [64]. Furthermore, dephosphorylation by VE-PTP enhances VE-cadherin-mediated barrier integrity [62], and the dissociation of VE-cadherin from VE-PTP is necessary to the adhesion of immune cells onto endothelium [65]. Thus, phosphorylation of VE-cadherin regulates and maintains endothelial integrity. Here, we observed that *EGFL7* knockdown increased the parent vessel permeability in response to VEGF-A while decreasing the VE-cadherin basal phosphorylation levels of the Y685/Y731 residues and limited the phosphorylation of Y658/Y685/Y731 in response to VEGF-A. This indicates that endogenous EGFL7 maintains and regulates the phosphorylation of VE-cadherin at least on these tyrosine residues and therefore suggests that the increased permeability of *EGFL7*-knockdowned parent vessels is due to the lack of phosphorylation of VE-cadherin, at least in part.

VE-cadherin is also involved in more fundamental aspects of sprouting angiogenesis, such as VEGFR-2 activation, endothelial cell proliferation, lumen formation [66], endothelial junction remodeling and cell migration [67,68]. It is probable that the effects of EGFL7 on tip cell emergence during sprouting angiogenesis are linked to those observed on the localization and phosphorylation of VE-cadherin (Fig. 6B). These links need to be further investigated.

From a bioengineering point of view, microvessel-on-a-chip technology allows the creation and observation of vascular functions such as sprouting angiogenesis, with concomitant measurements of permeability in a reconstituted blood vessel in a 3D context. Using 3D microvessel model, it is also possible to study the effect of flow. The effect of flow onto 3D model is still debated; some previous studies reported that flow enhanced sprouting angiogenesis in 3D models [69], but other suggested it had limited effect [70]. Importantly, our results suggest that the effects of EGFL7 on endothelial integrity are independent from flow effects, furthermore supported by the fact that 2D experiment also showed clear differences between siCtrl- and siEGFL7-endothelial cells. However, the effect of flow is still valuable and shall be addressed in future works.

This study highlights the value of such a microvessel model to investigate the biological properties of vascular effectors in experimental conditions close to *in vivo* or *ex vivo* methods, with the added flexibility of *in vitro* methods. For further analysis of cell–cell junctions, we were still able to combine this 3D model with more conventional 2D cell culture techniques in order to analyze the phosphorylation of VE-cadherin. In regard of cancer therapy, our model may facilitate the early evaluation of anti-EGFL7 antibodies as an anti-angiogenic treatment. Indeed, an anti-EGFL7 antibody was shown to enhance stress-induced endothelial cell death and anti-VEGF antibody efficacy [71]. Thereafter, this anti-EGFL7 antibody was clinically tested as a first-line treatment for metastatic colorectal cancer [72] and non-squamous non-small cell lung cancer [73], but these tests eventually failed at phase II. Our finding indicated that EGFL7 deficiency caused a loss of endothelial integrity through impaired VE-cadherin phosphorylation. This may be a reason for the poor clinical benefit brought by the anti-EGFL7 therapy and suggest leads to address existing issues.

5. Conclusion

The *in vitro* model enabled reproduction of some of the previously documented effects of *EGFL7* deficiency, but also led to the identification of unknown effects of EGFL7 on tip cell emergence and on endothelial integrity, providing further insight into EGFL7 function in endothelium. Although we uncovered functions of EGFL7, some questions remain unanswered. For example, we have not yet described the molecular mechanisms through which EGFL7 interfered with the phosphorylation of VE-cadherin or how it regulates the emergence of filopodia-rich tip-like cells in sprouting angiogenesis. Nevertheless, results from this study indicate that EGFL7 is an essential factor in the maintenance of adherens junctions in the context of inflammation and sprouting angiogenesis, and that it may interact with kinases/phosphatases involved in these processes. The present microvessel model facilitated (i) the study of gene knocked-down endothelial cells at a tissue level via a simple and convenient methods, (ii) the use of imaging and analysis methods to study sprouting angiogenesis, and (iii) the use of permeability/immune cell adhesion assays and immunofluorescence techniques for the study of endothelium. The *in vitro* microvessel model employed here demonstrated its capacity to enable elaborate observations for a better understanding of vascular biology.

Conflicts of interest

The authors declare no conflict of interests.

Acknowledgements

This work was partly supported by JSPS Overseas challenge Program for Young Researchers to R.U., Grant-in-Aid for JSPS Research Fellows, Grant for Specially Promoted Research by the Foundation for the Promotion of Industrial Science, and the Ligue Régionale contre le cancer and SFR Cancer Lille. R.U. is a Research Fellow of the JSPS. J.P. received a Fellowship for Research in Japan from the JSPS (P15767). F.S. is Directeur de Recherche of the Institut National de la Santé et de la Recherche Médicale. The authors thank Mr. Yasuhiro Ookawa and Dr. Koji Fujimoto (Dai Nippon Printing Co., Ltd.) for their assistance in the PDMS device fabrication, Dr. Yosuke Hiraoka (Nitta Gelatin Inc.) for his kind support in collagen preparation, Dr. Masayoshi Kobayashi, Mr. Keisuke Kato, Mr. Kenji Ueyama (SCREEN Holdings Co., Ltd.) for their advice regarding OCT and Ms. Eri Otsuka (The University of Tokyo) for her technical assistance.

Appendix A. Supplementary data

Supplementary data to this article can be found online at https://doi.org/10.1016/j.biomaterials.2019.01.022.

References

[1] P. Carmeliet, R.K. Jain, Molecular mechanisms and clinical applications of angiogenesis, Nature 473 (7347) (2011) 298–307.
[2] R.K. Jain, Normalization of tumor vasculature: an emerging concept in anti-angiogenic therapy, Science 307 (5706) (2005) 58–62.
[3] A. Rubsam, S. Parikh, P.E. Fort, Role of inflammation in diabetic retinopathy, Int. J. Mol. Sci. 19 (4) (2018) 942.
[4] A. Uemura, Pharmacologic management of diabetic retinopathy, J. Biochem. 163 (1) (2018) 3–9.
[5] M. Potente, H. Gerhardt, P. Carmeliet, Basic and therapeutic aspects of angiogenesis, Cell 146 (6) (2011) 873–887.
[6] D. Ribatti, E. Crivellato, "Sprouting angiogenesis", a reappraisal, Dev. Biol. 372 (2) (2012) 157–165.
[7] H. Gerhardt, M. Golding, M. Fruttiger, C. Ruhrberg, A. Lundkvist, A. Abramsson, M. Jeltsch, C. Mitchell, K. Alitalo, D. Shima, C. Betsholtz, VEGF guides angiogenic sprouting utilizing endothelial tip cell filopodia, J. Cell Biol. 161 (6) (2003) 1163–1177.
[8] M. Hellstrom, L.K. Phng, J.J. Hofmann, E. Wallgard, L. Coultas, P. Lindblom, J. Alva, A.K. Nilsson, L. Karlsson, N. Gaiano, K. Yoon, J. Rossant, M.L. Iruela-Arispe, M. Kalen, H. Gerhardt, C. Betsholtz, Dll4 signalling through Notch1 regulates formation of tip cells during angiogenesis, Nature 445 (7129) (2007) 776–780.
[9] G. Eelen, P. de Zeeuw, L. Treps, U. Harjes, B.W. Wong, P. Carmeliet, Endothelial cell metabolism, Physiol. Rev. 98 (1) (2018) 3–58.
[10] J.J. Mack, M.L. Iruela-Arispe, NOTCH regulation of the endothelial cell phenotype, Curr. Opin. Hematol. 25 (3) (2018) 212–218.
[11] H.W. Jeong, B. Hernandez-Rodriguez, J. Kim, K.P. Kim, R. Enriquez-Gasca, J. Yoon, S. Adams, H.R. Scholer, J.M. Vaquerizas, R.H. Adams, Transcriptional regulation of endothelial cell behavior during sprouting angiogenesis, Nat. Commun. 8 (2017) 726.
[12] F. Soncin, V. Mattot, F. Lionneton, N. Spruyt, F. Lepretre, A. Begue, D. Stehelin, VE-statin, an endothelial repressor of smooth muscle cell migration, EMBO J. 22 (21) (2003) 5700–5711.
[13] M.J. Fitch, L. Campagnolo, F. Kuhnert, H. Stuhlmann, Egfl7, a novel epidermal growth factor-domain gene expressed in endothelial cells, Dev. Dynam. 230 (2) (2004) 316–324.
[14] L.H. Parker, M. Schmidt, S.W. Jin, A.M. Gray, D. Beis, T. Pham, G. Frantz, S. Palmieri, K. Hillan, D.Y. Stainier, F.J. De Sauvage, W. Ye, The endothelial-cell-derived secreted factor Egfl7 regulates vascular tube formation, Nature 428 (6984) (2004) 754–758.
[15] M.S. Charpentier, K.S. Christine, N.M. Amin, K.M. Dorr, E.J. Kushner, V.L. Bautch, J.M. Taylor, F.L. Conlon, CASZ1 promotes vascular assembly and morphogenesis through the direct regulation of an EGFL7/RhoA-mediated pathway, Dev. Cell 25 (2) (2013) 132–143.
[16] D. Nichol, C. Shawber, M.J. Fitch, K. Bambino, A. Sharma, J. Kitajewski, H. Stuhlmann, Impaired angiogenesis and altered Notch signaling in mice overexpressing endothelial Egfl7, Blood 116 (26) (2010) 6133–6143.
[17] A. Durrans, H. Stuhlmann, A role for Egfl7 during endothelial organization in the embryoid body model system, J. Angiogenes Res. 2 (2010) 4.
[18] C. d'Audigier, S. Susen, A. Blandinieres, V. Mattot, B. Saubamea, E. Rossi, N. Nevo, S. Lecourt, C.L. Guerin, B. Dizier, N. Gendron, B. Caetano, P. Gaussem, F. Soncin, D.M. Smadja, Egfl7 represses the vasculogenic potential of human endothelial progenitor cells, Stem Cell Rev. 14 (1) (2018) 82–91.
[19] E. Lelievre, A. Hinek, F. Lupu, C. Buquet, F. Soncin, V. Mattot, VE-statin/egfl7 regulates vascular elastogenesis by interacting with lysyl oxidases, EMBO J. 27 (12) (2008) 1658–1670.
[20] G. Villain, E. Lelievre, T. Broekelmann, O. Gayet, C. Havet, E. Werkmeister, R. Mecham, N. Dusetti, F. Soncin, V. Mattot, MAGP-1 and fibronectin control EGFL7 functions by driving its deposition into distinct endothelial extracellular matrix locations, FEBS J. 285 (23) (2018) 4394–4412.
[21] R. Diaz, J. Silva, J.M. Garcia, Y. Lorenzo, V. Garcia, C. Pena, R. Rodriguez, C. Munoz, F. Garcia, F. Bonilla, G. Dominguez, Deregulated expression of miR-106a predicts survival in human colon cancer patients, Genes Chromosomes Cancer 47 (9) (2008) 794–802.
[22] F. Wu, L.Y. Yang, Y.F. Li, D.P. Ou, D.P. Chen, C. Fan, Novel role for epidermal growth factor-like domain 7 in metastasis of human hepatocellular carcinoma, Hepatology 50 (6) (2009) 1839–1850.
[23] C.H. Huang, X.J. Li, Y.Z. Zhou, Y. Luo, C. Li, X.R. Yuan, Expression and clinical significance of EGFL7 in malignant glioma, J. Canc. Res. Clin. Oncol. 136 (11) (2010) 1737–1743.
[24] S. Delfortrie, S. Pinte, V. Mattot, C. Samson, G. Villain, B. Caetano, G. Lauridant-Philippin, M.C. Baranzelli, J. Bonneterre, F. Trottein, C. Faveeuw, F. Soncin, Egfl7 promotes tumor escape from immunity by repressing endothelial cell activation, Cancer Res. 71 (23) (2011) 7176–7186.
[25] S. Pinte, B. Caetano, A. Le Bras, C. Havet, G. Villain, R. Dernayka, C. Duez, V. Mattot, F. Soncin, Endothelial cell activation is regulated by epidermal growth factor-like domain 7 (Egfl7) during inflammation, J. Biol. Chem. 291 (46) (2016) 24017–24028.
[26] A.M. Ghaemmaghami, M.J. Hancock, H. Harrington, H. Kaji, A. Khademhosseini, Biomimetic tissues on a chip for drug discovery, Drug Discov. Today 17 (3–4) (2012) 173–181.
[27] S.N. Bhatia, D.E. Ingber, Microfluidic organs-on-chips, Nat. Biotechnol. 32 (8) (2014) 760–772.
[28] S. Kim, H. Lee, M. Chung, N.L. Jeon, Engineering of functional, perfusable 3D microvascular networks on a chip, Lab Chip 13 (8) (2013) 1489–1500.
[29] Y. Zheng, J. Chen, M. Craven, N.W. Choi, S. Totorica, A. Diaz-Santana, P. Kermani, B. Hempstead, C. Fischbach-Teschl, J.A. Lopez, A.D. Stroock, In vitro microvessels for the study of angiogenesis and thrombosis, Proc. Natl. Acad. Sci. U. S. A 109 (24) (2012) 9342–9347.
[30] M. Campisi, Y. Shin, T. Osaki, C. Hajal, V. Chiono, R.D. Kamm, 3D self-organized microvascular model of the human blood-brain barrier with endothelial cells, pericytes and astrocytes, Biomaterials 180 (2018) 117–129.
[31] J. Pauty, R. Usuba, H. Takahashi, J. Suehiro, K. Fujisawa, K. Yano, T. Nishizawa, Y.T. Matsunaga, A vascular permeability assay using an in vitro human microvessel model mimicking the inflammatory condition, Nanotheranostics 1 (1) (2017) 103–113.
[32] J. Pauty, R. Usuba, I.G. Cheng, L. Hespel, H. Takahashi, K. Kato, M. Kobayashi, H. Nakajima, E. Lee, F. Yger, F. Soncin, Y.T. Matsunaga, A vascular endothelial growth factor-dependent sprouting angiogenesis assay based on an in vitro human blood vessel model for the study of anti-angiogenic drugs, EBioMedicine 27 (2018) 225–236.
[33] H. Takahashi, K. Kato, K. Ueyama, M. Kobayashi, G. Baik, Y. Yukawa, J.I. Suehiro, Y.T. Matsunaga, Visualizing dynamics of angiogenic sprouting from a three-dimensional microvasculature model using stage-top optical coherence tomography, Sci. Rep. 7 (2017) 42426.
[34] Y. Yokota, H. Nakajima, Y. Wakayama, A. Muto, K. Kawakami, S. Fukuhara, N. Mochizuki, Endothelial Ca 2+ oscillations reflect VEGFR signaling-regulated angiogenic capacity in vivo, Elife 4 (2015) e08817.
[35] M.H.H. Schmidt, F. Bicker, I. Nikolic, J. Meister, T. Babuke, S. Picuric, W. Muller-Esterl, K.H. Plate, I. Dikic, Epidermal growth factor-like domain 7 (EGFL7) modulates Notch signalling and affects neural stem cell renewal, Nat. Cell Biol. 11 (7) (2009) 873–880.
[36] I. Spyridopoulos, C. Luedemann, D. Chen, M. Kearney, D. Chen, T. Murohara, N. Principe, J.M. Isner, D.W. Losordo, Divergence of angiogenic and vascular permeability signaling by VEGF, Arterioscler. Thromb. Vasc. Biol. 22 (6) (2002) 901–906.
[37] C. Weber, L. Fraemohs, E. Dejana, The role of junctional adhesion molecules in vascular inflammation, Nat. Rev. Immunol. 7 (6) (2007) 467–477.
[38] D. Vestweber, VE-cadherin: the major endothelial adhesion molecule controlling cellular junctions and blood vessel formation, Arterioscler. Thromb. Vasc. Biol. 28 (2) (2008) 223–232.
[39] J. Gavard, J.S. Gutkind, VEGF controls endothelial-cell permeability by promoting the beta-arrestin-dependent endocytosis of VE-cadherin, Nat. Cell Biol. 8 (11) (2006) 1223–1234.
[40] K. Noda, J. Zhang, S. Fukuhara, S. Kunimoto, M. Yoshimura, N. Mochizuki, Vascular endothelial-cadherin stabilizes at cell-cell junctions by anchoring to circumferential actin bundles through alpha- and beta-catenins in cyclic AMP-Epac-Rap 1 signal-activated endothelial cells, Mol. Biol. Cell 21 (4) (2010) 584–596.
[41] C. Larochelle, T. Uphaus, B. Broux, E. Gowing, M. Paterka, L. Michel, N. Dudvarski Stankovic, F. Bicker, F. Lemaitre, A. Prat, M.H.H. Schmidt, F. Zipp, EGFL7 reduces CNS inflammation in mouse, Nat. Commun. 9 (2018) 819.
[42] P.L. Hordijk, E. Anthony, F.P. Mul, R. Rientsma, L.C. Oomen, D. Roos, Vascular-endothelial-cadherin modulates endothelial monolayer permeability, J. Cell Sci. 112 (Pt 12) (1999) 1915–1923.
[43] E.S. Harris, W.J. Nelson, VE-cadherin: at the front, center, and sides of endothelial cell organization and function, Curr. Opin. Cell Biol. 22 (5) (2010) 651–658.
[44] D. Mehta, A.B. Malik, Signaling mechanisms regulating endothelial permeability, Physiol. Rev. 86 (1) (2006) 279–367.
[45] F. Orsenigo, C. Giampietro, A. Ferrari, M. Corada, A. Galaup, S. Sigismund, G. Ristagno, L. Maddaluno, G.Y. Koh, D. Franco, V. Kurtcuoglu, D. Poulikakos, P. Baluk, D. McDonald, M. Grazia Lampugnani, E. Dejana, Phosphorylation of VE-cadherin is modulated by haemodynamic forces and contributes to the regulation of

vascular permeability in vivo, Nat. Commun. 3 (2012) 1208.
[46] E. Monaghan-Benson, K. Burridge, The regulation of vascular endothelial growth factor-induced microvascular permeability requires Rac and reactive oxygen species, J. Biol. Chem. 284 (38) (2009) 25602–25611.
[47] J. Welti, S. Loges, S. Dimmeler, P. Carmeliet, Recent molecular discoveries in angiogenesis and antiangiogenic therapies in cancer, J. Clin. Invest. 123 (8) (2013) 3190–3200.
[48] S. Selvam, T. Kumar, M. Fruttiger, Retinal vasculature development in health and disease, Prog. Retin. Eye Res. 63 (2018) 1–19.
[49] A. Beenken, M. Mohammadi, The FGF family: biology, pathophysiology and therapy, Nat. Rev. Drug Discov. 8 (3) (2009) 235–253.
[50] M. Murakami, L.T. Nguyen, Z.W. Zhuang, K.L. Moodie, P. Carmeliet, R.V. Stan, M. Simons, The FGF system has a key role in regulating vascular integrity, J. Clin. Invest. 118 (10) (2008) 3355–3366.
[51] H.J. Joo, S. Song, H.R. Seo, J.H. Shin, S.C. Choi, J.H. Park, C.W. Yu, S.J. Hong, D.S. Lim, Human endothelial colony forming cells from adult peripheral blood have enhanced sprouting angiogenic potential through up-regulating VEGFR2 signaling, Int. J. Cardiol. 197 (2015) 33–43.
[52] D. Tasev, L.S. Konijnenberg, J. Amado-Azevedo, M.H. van Wijhe, P. Koolwijk, V.W. van Hinsbergh, CD34 expression modulates tube-forming capacity and barrier properties of peripheral blood-derived endothelial colony-forming cells (ECFCs), Angiogenesis 19 (3) (2016) 325–338.
[53] M. Schmidt, K. Paes, A. De Maziere, T. Smyczek, S. Yang, A. Gray, D. French, I. Kasman, J. Klumperman, D.S. Rice, W. Ye, EGFL7 regulates the collective migration of endothelial cells by restricting their spatial distribution, Development 134 (16) (2007) 2913–2923.
[54] D. Stenzel, C.A. Franco, S. Estrach, A. Mettouchi, D. Sauvaget, I. Rosewell, A. Schertel, H. Armer, A. Domogatskaya, S. Rodin, K. Tryggvason, L. Collinson, L. Sorokin, H. Gerhardt, Endothelial basement membrane limits tip cell formation by inducing Dll4/Notch signalling in vivo, EMBO Rep. 12 (11) (2011) 1135–1143.
[55] A. Fantin, J.M. Vieira, A. Plein, L. Denti, M. Fruttiger, J.W. Pollard, C. Ruhrberg, NRP1 acts cell autonomously in endothelium to promote tip cell function during sprouting angiogenesis, Blood 121 (12) (2013) 2352–2362.
[56] I. Geudens, H. Gerhardt, Coordinating cell behaviour during blood vessel formation, Development 138 (21) (2011) 4569–4583.
[57] L. Jakobsson, C.A. Franco, K. Bentley, R.T. Collins, B. Ponsioen, I.M. Aspalter, I. Rosewell, M. Busse, G. Thurston, A. Medvinsky, S. Schulte-Merker, H. Gerhardt, Endothelial cells dynamically compete for the tip cell position during angiogenic sprouting, Nat. Cell Biol. 12 (10) (2010) 943–953.
[58] L.K. Phng, F. Stanchi, H. Gerhardt, Filopodia are dispensable for endothelial tip cell guidance, Development 140 (19) (2013) 4031–4040.
[59] M.G. Lampugnani, A novel endothelial-specific membrane protein is a marker of cell-cell contacts, J. Cell Biol. 118 (6) (1992) 1511–1522.
[60] U. Gotsch, E. Borges, R. Bosse, E. Boggemeyer, M. Simon, H. Mossmann, D. Vestweber, VE-cadherin antibody accelerates neutrophil recruitment in vivo, J. Cell Sci. 110 (Pt 5) (1997) 583–588.
[61] M. Corada, M. Mariotti, G. Thurston, K. Smith, R. Kunkel, M. Brockhaus, M.G. Lampugnani, I. Martin-Padura, A. Stoppacciaro, L. Ruco, D.M. McDonald, P.A. Ward, E. Dejana, Vascular endothelial-cadherin is an important determinant of microvascular integrity in vivo, Proc. Natl. Acad. Sci. U. S. A 96 (17) (1999) 9815–9820.
[62] R. Nawroth, G. Poell, A. Ranft, S. Kloep, U. Samulowitz, G. Fachinger, M. Golding, D.T. Shima, U. Deutsch, D. Vestweber, VE-PTP and VE-cadherin ectodomains interact to facilitate regulation of phosphorylation and cell contacts, EMBO J. 21 (18) (2002) 4885–4895.
[63] F. Wessel, M. Winderlich, M. Holm, M. Frye, R. Rivera-Galdos, M. Vockel, R. Linnepe, U. Ipe, A. Stadtmann, A. Zarbock, A.F. Nottebaum, D. Vestweber, Leukocyte extravasation and vascular permeability are each controlled in vivo by different tyrosine residues of VE-cadherin, Nat. Immunol. 15 (3) (2014) 223–230.
[64] A. Sidibe, H. Polena, K. Pernet-Gallay, J. Razanajatovo, T. Mannic, N. Chaumontel, S. Bama, I. Marechal, P. Huber, D. Gulino-Debrac, L. Bouillet, I. Vilgrain, VE-cadherin Y685F knock-in mouse is sensitive to vascular permeability in recurrent angiogenic organs, Am. J. Physiol. Heart Circ. Physiol. 307 (3) (2014) H455–H463.
[65] A. Broermann, M. Winderlich, H. Block, M. Frye, J. Rossaint, A. Zarbock, G. Cagna, R. Linnepe, D. Schulte, A.F. Nottebaum, D. Vestweber, Dissociation of VE-PTP from VE-cadherin is required for leukocyte extravasation and for VEGF-induced vascular permeability in vivo, J. Exp. Med. 208 (12) (2011) 2393–2401.
[66] Y. Wallez, I. Vilgrain, P. Huber, Angiogenesis: the VE-cadherin switch, Trends Cardiovasc. Med. 16 (2) (2006) 55–59.
[67] K. Bentley, C.A. Franco, A. Philippides, R. Blanco, M. Dierkes, V. Gebala, F. Stanchi, M. Jones, I.M. Aspalter, G. Cagna, S. Westrom, L. Claesson-Welsh, D. Vestweber, H. Gerhardt, The role of differential VE-cadherin dynamics in cell rearrangement during angiogenesis, Nat. Cell Biol. 16 (4) (2014) 309–321.
[68] J. Cao, M. Ehling, S. März, J. Seebach, K. Tarbashevich, T. Sixta, M.E. Pitulescu, A.-C. Werner, B. Flach, E. Montanez, E. Raz, R.H. Adams, H. Schnittler, Polarized actin and VE-cadherin dynamics regulate junctional remodelling and cell migration during sprouting angiogenesis, Nat. Commun. 8 (1) (2017) 2210.
[69] P.A. Galie, D.H. Nguyen, C.K. Choi, D.M. Cohen, P.A. Janmey, C.S. Chen, Fluid shear stress threshold regulates angiogenic sprouting, Proc. Natl. Acad. Sci. U. S. A 111 (22) (2014) 7968–7973.
[70] J.W. Song, L.L. Munn, Fluid forces control endothelial sprouting, Proc. Natl. Acad. Sci. U. S. A 108 (37) (2011) 15342–15347.
[71] L. Johnson, M. Huseni, T. Smyczek, A. Lima, S. Yeung, J.H. Cheng, R. Molina, D. Kan, A. De Maziere, J. Klumperman, I. Kasman, Y. Zhang, M.S. Dennis, J. Eastham-Anderson, A.M. Jubb, O. Hwang, R. Desai, M. Schmidt, M.A. Nannini, K.H. Barck, R.A. Carano, W.F. Forrest, Q. Song, D.S. Chen, L. Naumovski, M. Singh, W. Ye, P.S. Hegde, Anti-EGFL7 antibodies enhance stress-induced endothelial cell death and anti-VEGF efficacy, J. Clin. Invest. 123 (9) (2013) 3997–4009.
[72] R. Garcia-Carbonero, E. van Cutsem, F. Rivera, J. Jassem, I. Gore Jr., N. Tebbutt, F. Braiteh, G. Argiles, Z.A. Wainberg, R. Funke, M. Anderson, B. McCall, M. Stroh, E. Wakshull, P. Hegde, W. Ye, D. Chen, I. Chang, I. Rhee, H. Hurwitz, Randomized phase II trial of parsatuzumab (Anti-EGFL7) or placebo in combination with FOLFOX and bevacizumab for first-line metastatic colorectal cancer, Oncologist 22 (4) (2017) 375-e30.
[73] J. von Pawel, D.R. Spigel, T. Ervin, G. Losonczy, F. Barlesi, E. Juhasz, M. Anderson, B. McCall, E. Wakshull, P. Hegde, W. Ye, D. Chen, I. Chang, I. Rhee, M. Reck, Randomized phase II trial of parsatuzumab (Anti-EGFL7) or placebo in combination with carboplatin, paclitaxel, and bevacizumab for first-line nonsquamous non-small cell lung cancer, Oncologist 23 (6) (2018) 654-e58.

Supplementary Data

EGFL7 regulates sprouting angiogenesis and endothelial integrity in a human blood vessel model

Ryo Usuba[a], Joris Pauty[a,b], Fabrice Soncin[b,c,d,*], Yukiko T. Matsunaga[a,b,c,*]

[a] Center for International Research on Integrative Biomedical Systems (CIBiS), Institute of Industrial Science, The University of Tokyo, 4-6-1 Komaba, Meguro-ku, Tokyo 153-8505, Japan

[b] LIMMS/CNRS-IIS (UMI 2820), Institute of Industrial Science, The University of Tokyo, 4-6-1 Komaba, Meguro-ku, Tokyo 153-8505, Japan

[c] CNRS/IIS/COL/Liile University SMMiL-E Project, CNRS Délégation Nord-Pas de Calais et Picardie, 2 rue de Canonniers, Lille, Cedex 59046, France

[d] Université de Lille, CNRS, Institut Pasteur de Lille, UMR 8161 - M3T, F-59000 Lille, France

*Corresponding authors:

Yukiko T. Matsunaga, Ph.D.

Institute of Industrial Science, The University of Tokyo 4-6-1 Komaba, Meguro-ku, Tokyo 153-8505, Japan
Tel.: +81-3-5452–6470; Fax: +81-3-5452-6471 E-mail: mat@iis.u-tokyo.ac.jp

Fabrice Soncin, Ph.D.

CNRS UMI2820 LIMMS-IIS – SMMiL-E Project, IRCL, Place de Verdun, 59045 Lille, France
E-mail: fabrice.soncin@inserm.fr

Table of Contents

Supplementary Method. Immunohistochemistry (IHC) analysis of the microvessel

The microvessels were fixed with 4% PFA overnight and then paraffinized with Paraplast (#15159-409, Mccormick). The blocks were sectioned at 8 μm, and sections were attached on a glass slide (#PRO-02, Matsunami) and deparaffinized. The sections were then blocked with PBS, 1% BSA, 5% goat serum (blocking solution) for 30 minutes at 25°C, and incubated overnight at 4°C with primary antibody in blocking solution (anti collagen IV (1:200, rabbit pAb, ab6586, Abcam) and anti CD31 (1:200, mouse mAb, M0823, Dako)). After washing with PBS, sections were incubated for 2 hours at 25°C with a secondary antibody (1:400, Alexa Fluor 568 goat anti-rabbit, Alexa Fluor 488 goat anti-mouse antibodies). After further washes with PBS, nuclei were stained by incubating the sections for 15 minutes at 25°C with Hoechst 33342 (1:1000) in PBS. Finally, the sections were mounted with glycerol, and stored at 4°C until imaging.

Supplementary Table S1. TaqMan probes for quantitative real time PCR

Gene	Assay ID	Fluorophore
hB2M	Human B2M (beta-2-microglobulin) Endogenous Control	VIC/MGB probe , primer limited
hDLL4	Hs00184092_m1	FAM/MGB
hEGFL7	Hs00211952_m1	FAM/MGB
hHES1	Hs00172878_m1	FAM/MGB
hHES2	Hs01021800_g1	FAM/MGB
hHEY1	Hs01114113_m1	FAM/MGB
hHEY2	Hs00232622_m1	FAM/MGB
hICAM-1	Hs00164932_m1	FAM/MGB
hJAG1	Hs01070032_m1	FAM/MGB
hNOTCH1	Hs01062014_m1	FAM/MGB
hNOTCH4	Hs00965889_m1	FAM/MGB
hNRP1	Hs00826128_m1	FAM/MGB
hNRP2	Hs00187290_m1	FAM/MGB
hVEGFR1	Hs01052961_m1	FAM/MGB
hVEGFR2	Hs00911700_m1	FAM/MGB

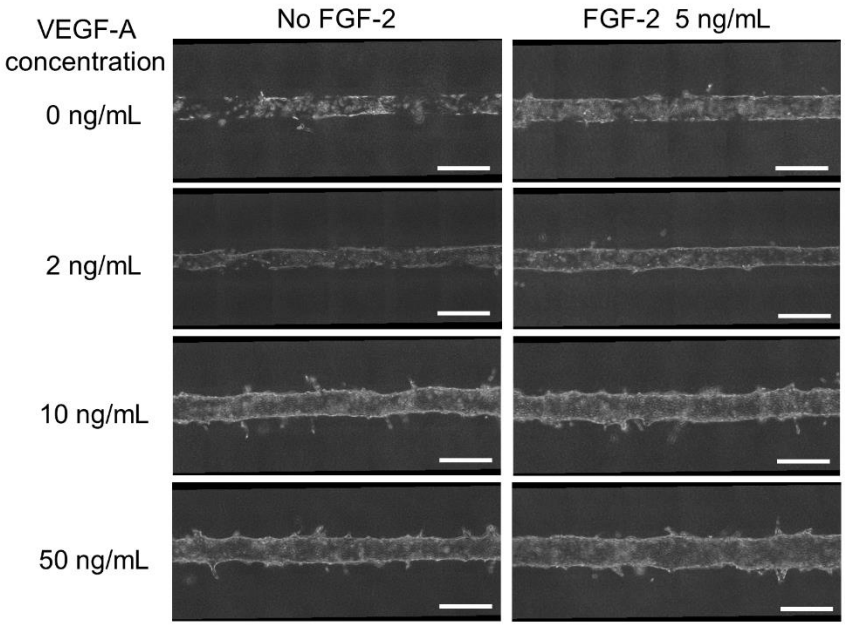

Figure S1. Optimization of VEGF-A and FGF-2 concentrations for a clear discrimination between quiescent state and VEGF-A-induced sprouting angiogenesis. Scale bar: 500 μm. FGF-2 was required to maintain quiescent microvessel in low VEGF-A media. Low concentration of VEGF-A improved cell survival. At a VEGF-A concentration of 10 ng/mL and above, the microvessel sprouted. Furthermore, the microvessel diameter increased with 10 and 50 ng/mL of VEGF-A, which may indicate cell proliferation.

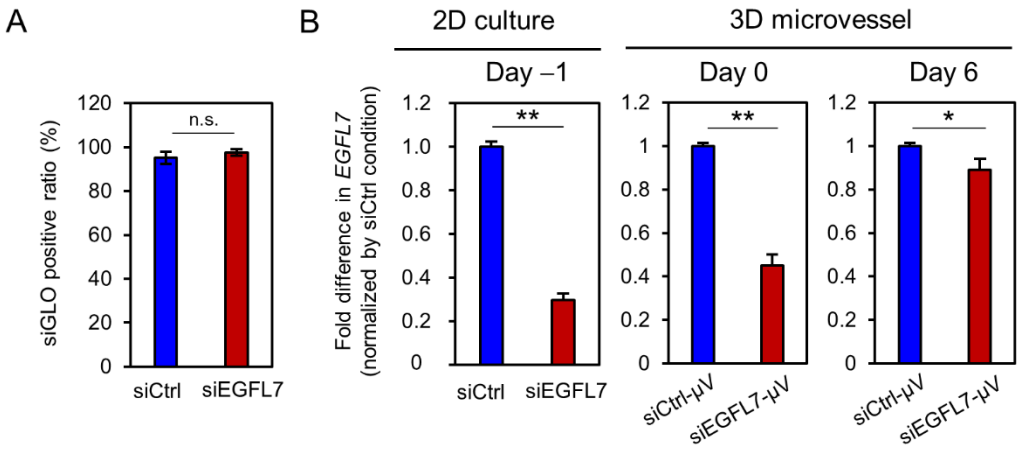

Figure S2. Transfection efficiency and knockdown efficiency of *EGFL7*. (A) Transfection efficiency estimated from the siGLO transfected HUVEC. A fluorescent siRNA transfection indicator, siGLO, was transfected along with siCtrl or siEGFL7. siGLO-positive-cell ratio was calculated from fluorescent images (n = 3). (B) Knockdown efficiency of *EGFL7*. For day -1 measurement and day 0 and 6 measurements, RNA was analyzed from 2D culture and 3D microvessels, respectively. Relative proportion of *EGFL7* compared to the beta-2 microglobulin gene as quantified by RT-qPCR; the value was normalized to the siCtrl condition and is expressed as a fold difference. Error bars = S.D. *$p < 0.05$; **$p < 0.01$.

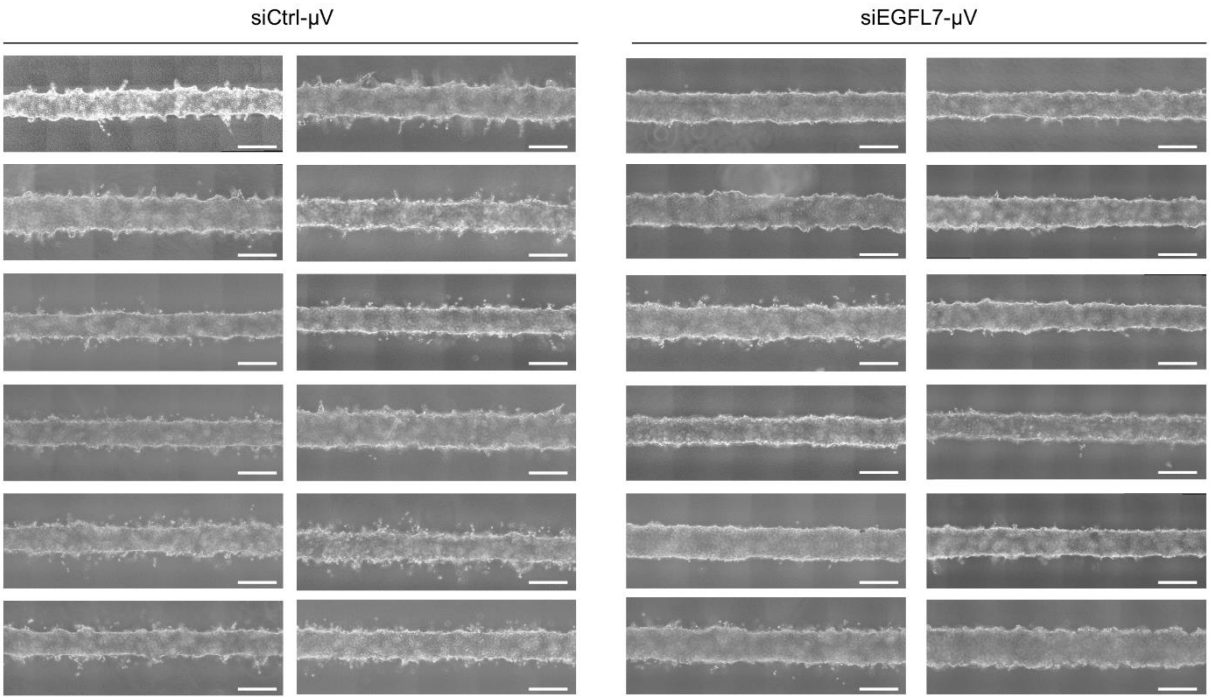

Figure S3. Images for sprouting angiogenesis induced by VEGF-A. Phase-contrast images of the siCtrl-μV and siEGFL7-μV cultured for 6 days in high-VEGF condition. Scale bar: 500 μm.

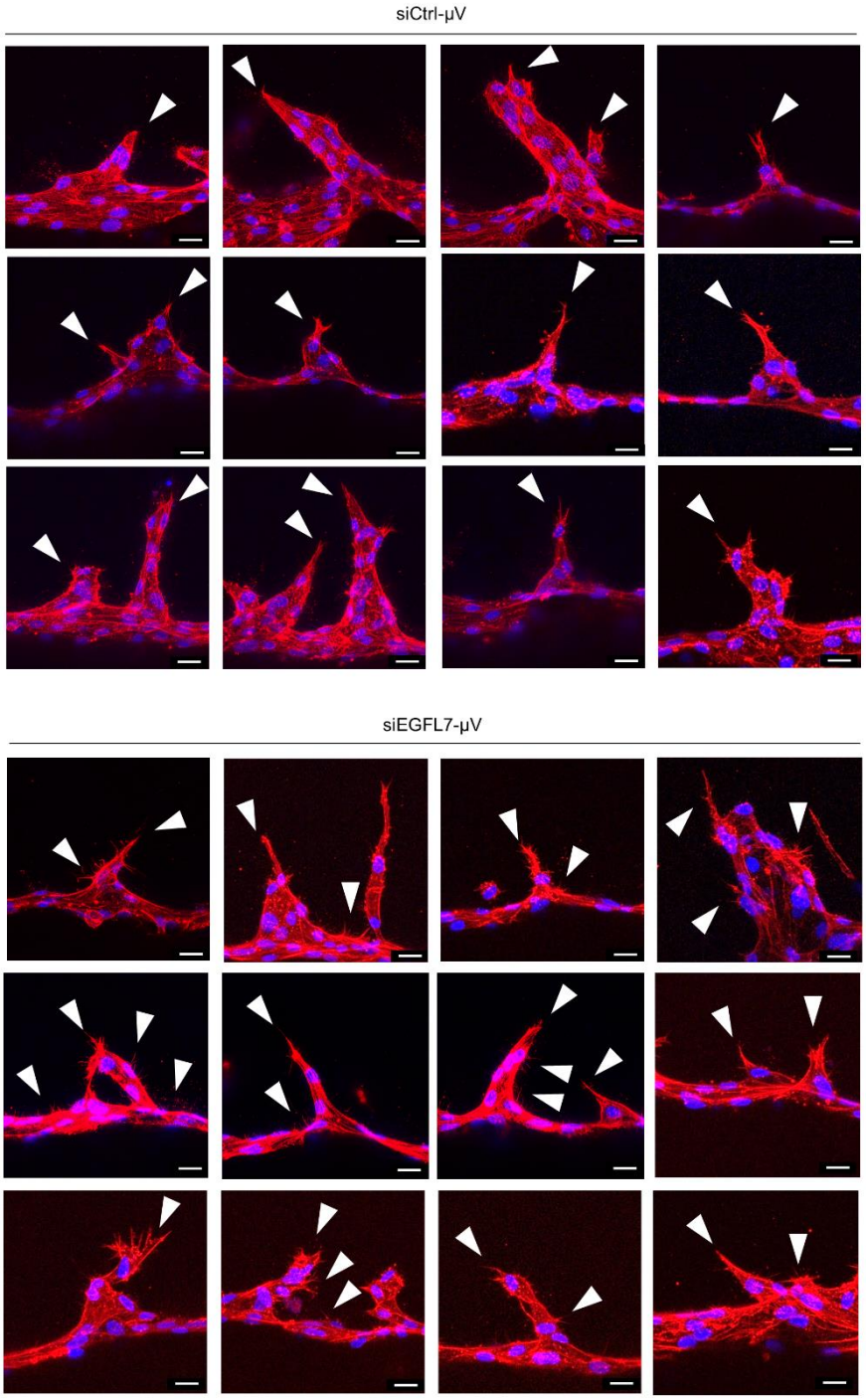

Figure S4. Images for VEGF-A-induced sprout in the microvessel. Fluorescence images of induced sprouts in the siCtrl-μV and siEGFL7-μV cultured for 4 days in high-VEGF condition. Induced sprouts were visualized by immunofluorescence under CLSM (red: F-actin, blue: nuclei). A white triangle indicates an area where filopodia elongated from an endothelial cell. Scale bar: 20 μm.

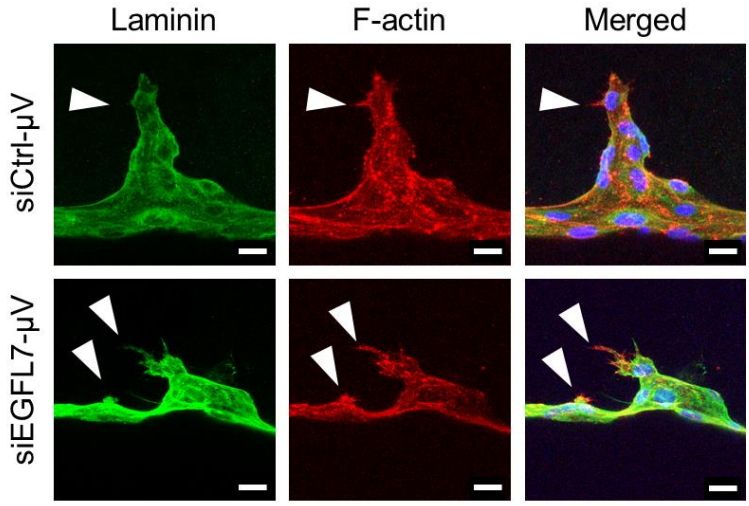

Figure S5. Immunofluorescence images of microvessels stained for laminin. The characterization of angiogenic sprouts were conducted for laminin by CLSM. White triangles indicate filopodia of tip-like cell that lack laminin. Scale bar: 20 μm.

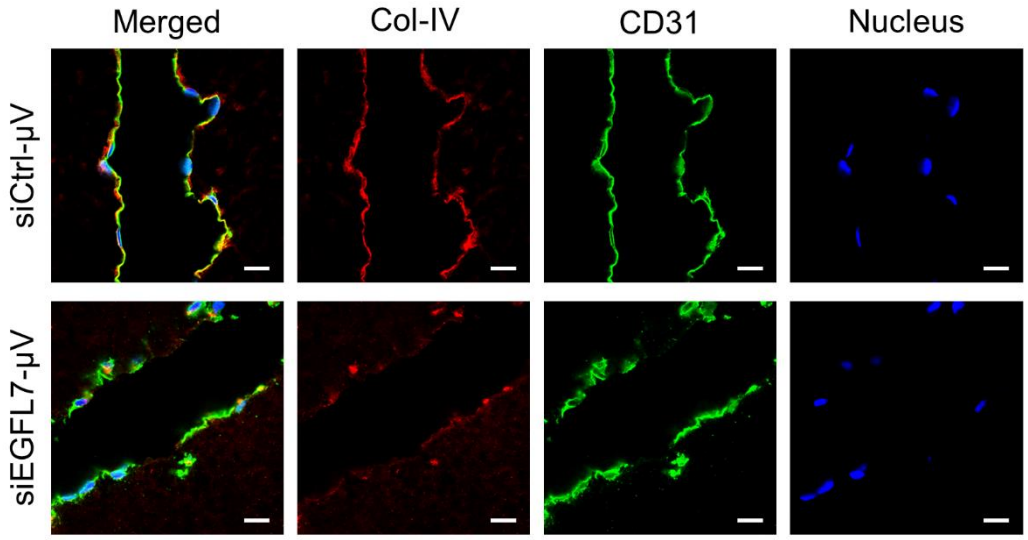

Figure S6. Immunohistochemistry images of microvessels stained for collagen IV (Col-IV), the endothelial cell marker CD31, and nuclei. Scale bar: 20 μm.